Precision Placement of DNA Origami onto Patterned Silicon Wafer Surfaces

Leo Huang
Yunjeong Park, Ed.
Grigory Tikhomirov, Ed.

Electrical Engineering and Computer Sciences
University of California, Berkeley

Technical Report No. UCB/EECS-2025-76
http://www2.eecs.berkeley.edu/Pubs/TechRpts/2025/EECS-2025-76.html

May 15, 2025

Precision Placement of DNA Origami onto Patterned Silicon Wafer Surfaces

Leo Huang

Research Project

Submitted to the Department of Electrical Engineering and Computer Sciences, University of California at Berkeley, in partial satisfaction of the requirements for the degree of **Master of Science, Plan II**.

Approval for the Report and Comprehensive Examination:

Committee:

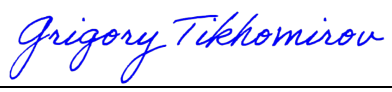

Professor Grigory Tikhomirov
Research Advisor

5/14/2025

(Date)

* * * * * * *

Professor Boubacar Kanté
Second Reader

05/14/2025

(Date)

Precision Placement of DNA Origami onto Patterned Silicon Wafer Surfaces

by

Leo Huang

A thesis submitted in partial satisfaction of the

requirements for the degree of

Masters of Science

in

Electrical Engineering and Computer Science

in the

Graduate Division

of the

University of California, Berkeley

Committee in charge:

Professor Grigory Tikhomirov, Chair
Professor Boubacar Kanté

Spring 2025

Precision Placement of DNA Origami onto Patterned Silicon Wafer Surfaces

Abstract

Precision Placement of DNA Origami onto Patterned Silicon Wafer Surfaces

by

Leo Huang

Masters of Science in Electrical Engineering and Computer Science

University of California, Berkeley

Professor Grigory Tikhomirov, Chair

Structural DNA nanotechnology offers a promising route for constructing nanometer-scale components with high spatial precision, while top-down photolithographic techniques remain essential for producing patterned substrates at scale. Previous work – most notably by Gopinath et al. – has demonstrated precise placement of DNA origami using electron beam lithography, but this approach's low throughput poses challenges for broader application. Here, we extend this approach by exploring the use of fractal-assembled DNA origami tiles for site-specific deposition onto photolithographically patterned silicon surfaces. This work initiates a systematic exploration of how tile geometry, surface chemistry, and binding conditions influence the integration of DNA nanostructures with scalable fabrication platforms, specifically their impact on placement yield and quality. Our work compares electrostatically and thermodynamically driven binding strategies as a step towards a more generalizable framework for hybrid bottom-up/top-down nanofabrication methods. We envision this method to complement existing approaches and expand the role of DNA origami in applications such as biosensing and programmable nanosystems.

To my friends and family,

Contents

List of Figures

List of Tables

Acknowledgments

I want to thank Professor Grigory Tikhomirov for his continued support and feedback throughout my years working with him. I would also like to thank my mentors, Professor Lin Du and Dr. Yunjeong Park, who have offered me incredible guidance and help throughout my research journey. Finally, I would like to thank my friends and family, whose warmth and support have pushed me to be who I am today.

Chapter 1

Introduction

DNA origami has rapidly advanced as a promising platform for constructing nanometer-scale structures with exceptional geometric precision and design flexibility. By leveraging the programmable base-pairing of DNA strands, it is possible to assemble arbitrary 2D and 3D architectures with sub-nanometer control, enabling applications in molecular computation, nanoscale patterning, and biosensing. However, despite significant progress in creating increasingly complex structures – from single-unit designs to large pixel-addressable arrays through hierarchical and fractal assembly – the broader integration of DNA origami into scalable fabrication workflows remains an open challenge. As DNA nanotechnology moves toward more intricate systems, reliably positioning and aligning these structures on solid substrates becomes increasingly critical, particularly for those requiring high-throughput, site-specific deposition.

Recent advances in scalable assembly strategies, such as fractal and hierarchical tiling, have significantly expanded the design space of DNA origami. These approaches enable the generation of large, pixel-addressable arrays from a small set of modular components, allowing for increasingly complex and spatially extensive DNA nanostructures. This ability to produce intricate, programmable assemblies positions DNA origami as a versatile platform for molecular computation, nanoscale patterning, and sensing. However, as these structures grow in scale and functional diversity, the challenge shifts from assembly to integration, specifically, how to transfer these assemblies onto solid substrates with high spatial fidelity and reproducibility.

Beyond programmable shapes, methods for reliably positioning DNA nanostructures on conventional substrates with high yield, spatial accuracy, and pattern diversity can further extend the applications of DNA nanotechnology. One promising approach is to guide DNA origami to bind site-specifically onto chemically defined regions of a silicon surface. Prior work has demonstrated that lithographically patterned binding sites, particularly those defined via electron beam lithography, can achieve high-precision placement of origami structures. This capability has enabled compelling proof-of-concept devices, such as nanophotonic resonators with emitter-origami coupling and large-scale DNA nanoarrays for molecular patterning. However, reliance on electron beam lithography presents a scalability bottleneck.

Its limited throughput, high cost, and serial nature make it poorly suited for integration with wafer-scale or commercial manufacturing processes.

This thesis explores an alternative strategy for DNA origami placement that combines large-scale fractal assembly of DNA nanostructures with high-throughput photolithographic patterning of silicon substrates. Fractal-assembled origami enables the construction of large, addressable DNA arrays from modular components, serving as a scalable bottom-up fabrication strategy. Meanwhile, photolithography provides an accessible, industry-standard method for defining placement sites across large areas. Together, these approaches present new opportunities for hybrid bottom-up/top-down fabrication, bridging the nanoscale precision of DNA assembly with the scalability of semiconductor manufacturing.

Here, we systematically investigate how origami tile geometry, surface chemistry, and binding modality affect placement performance, specifically yield and bond quality. We compare electrostatically mediated binding to thermodynamically controlled hybridization schemes and evaluate how different tile designs interact with photolithographically patterned features. We aim to establish a more generalizable framework for integrating complex DNA nanostructures with scalable substrate fabrication techniques. Ultimately, we envision this methodology complementing existing approaches and contributing toward the broader adoption of DNA-based components in biosensing, nanoscale patterning, and programmable molecular systems.

Chapter 2

Background and Related Work

2.1 Introduction to DNA Origami and Nanotechnology

DNA origami, first introduced by Rothemund [6], enables the folding of a long single-stranded DNA into well-defined nanoscale shapes using complementary short staple strands, resulting in precise programmable nanoscale assemblies with high yield and geometric homogeneity. This technique has evolved to produce 2D and 3D structures capable of complex molecular organization, serving as scaffolds for functional molecules, nanoparticles, and biomolecules. Applications span from biosensing and molecular computing to targeted drug delivery systems, showcasing the versatile programmability of DNA origami [3]. Structural DNA nanotechnology thus bridges molecular self-assembly with top-down lithographic techniques, offering new avenues for nanoscale patterning and device fabrication.

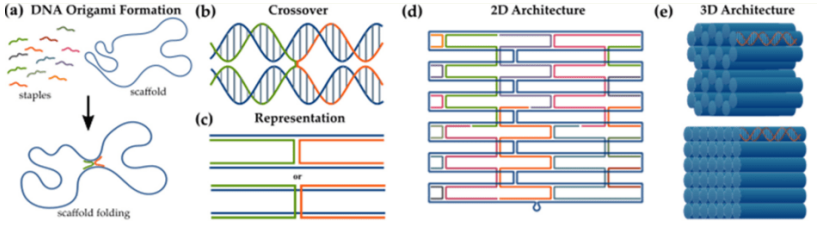

(a) Adapted figure from Babatunde et al. [1] illustrating DNA origami design.

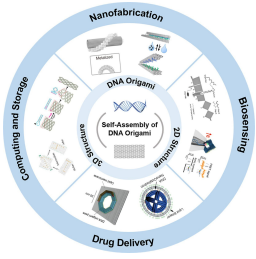

(b) Adapted figure from Zhimei et al. [3]

2.2 Previous Work on DNA Origami Placement

Both Ashwin Gopinath et al. [2] demonstrated a robust method for precisely placing DNA origami structures using electron beam lithography to define binding sites on silicon ni-

tride surfaces. This method achieved up to 94% placement yield, enabling the coupling of molecular emitters to photonic crystal cavities (PCCs) for enhanced light-matter interactions. The approach effectively utilized carboxylate-functionalized binding sites, allowing for the directed self-assembly of Cy5-labeled DNA origami, achieving spatial control crucial for nanophotonic and quantum information systems. However, the scalability of this technique remains constrained by the throughput limitations inherent in electron beam lithography.

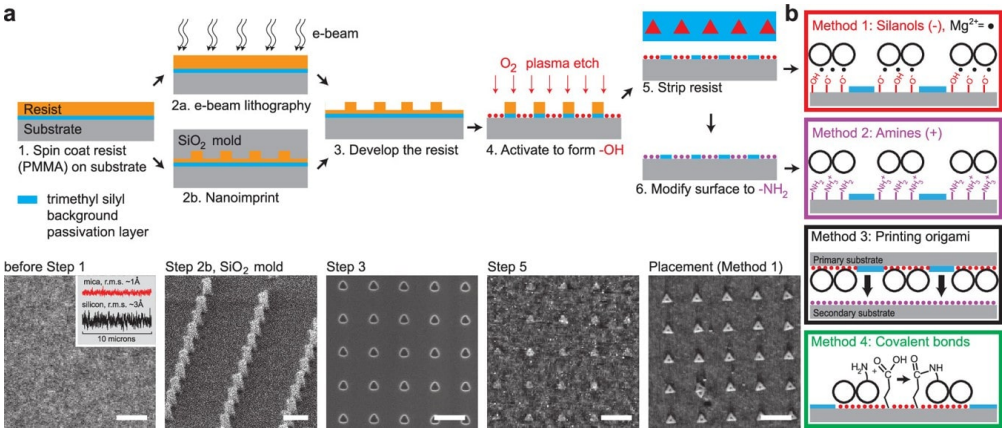

Figure 2.2: Adapted figure from Gopinath et a. [2] illustrating self-assembly of DNA origami on lithographically patterned surfaces.

Additionally, Kershner et al. [4] developed a technique for placing and orienting individual DNA origami structures on lithographically patterned surfaces. By employing electron-beam lithography and dry oxidative etching, they created binding sites on substrates like SiO_2 and diamond-like carbon that matched the shape of the DNA origami. This approach achieved high selectivity and orientation control, with 70–95% of the sites occupied by single DNA origami structures aligned within $\pm 10°$on diamond-like carbon and $\pm 20°$on SiO_2. Such precision is crucial for integrating DNA nanostructures into nanoelectronic and nano-optical devices, as it ensures consistent positioning and orientation necessary for device functionality. This work underscores the potential of combining top-down lithographic techniques with bottom-up DNA self-assembly to fabricate complex nanodevices.

2.3 Fractal Assembly and Large-Scale DNA Origami Patterns

Grigory Tikhomirov et al. [7] advanced the scalability of DNA origami assembly by introducing fractal assembly. This hierarchical assembly method constructs large-scale patterns using smaller DNA origami tiles as modular building blocks. By encoding binding interactions at each assembly stage, this method facilitated the generation of micrometer-scale patterns

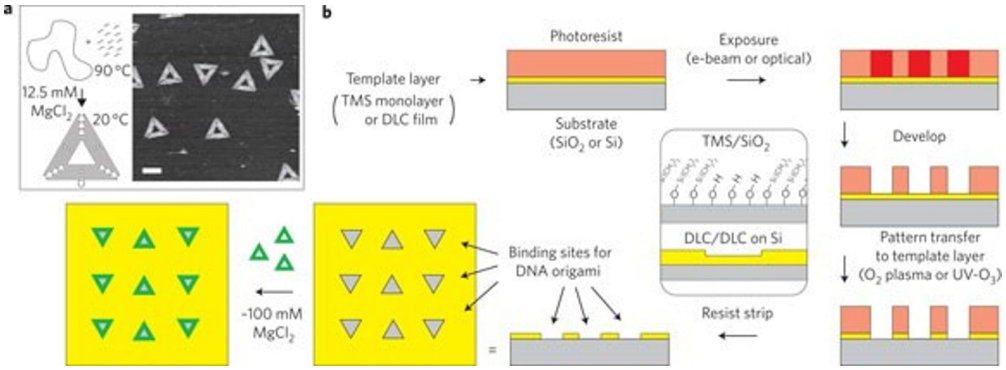

Figure 2.3: Adapted figure from Kershner et al. [4].

with up to 8,704 addressable pixels, expanding the potential for DNA nanostructures to integrate with larger substrate areas while maintaining nanoscale precision. The fractal assembly framework also demonstrated robustness in generating complex patterns without compromising spatial resolution, underscoring its applicability in creating programmable DNA-based materials.

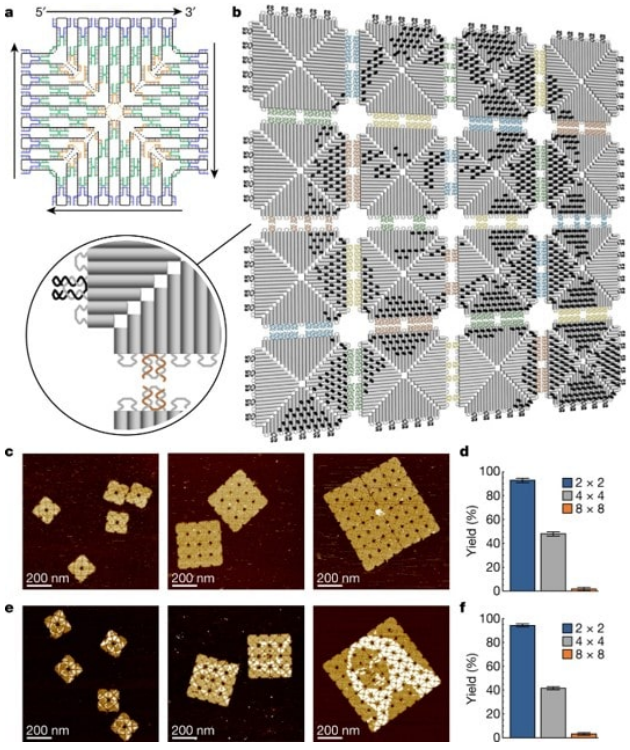

Figure 2.4: Adapted figure from Tikhomirov et al. [7] illustrating fractal assembly of DNA tiles.

2.4 Triangular DNA Origami Tiles and 3D Structures

In further work, Tikhomirov et al. [8] explored using triangular DNA origami tiles for two-dimensional and three-dimensional assemblies. Unlike previous square tile designs, these triangular tiles provided additional structural flexibility, allowing for controlled transitions between planar arrays and polyhedral structures. The researchers achieved tunable assembly modes by adjusting parameters such as tile concentration and magnesium ion content, producing both extended 2D arrays and compact 3D rhombic triacontahedrons. This approach introduced new geometric configurations for DNA origami, enabling the development of more complex, reconfigurable DNA nanostructures that could interface with lithographically patterned surfaces.

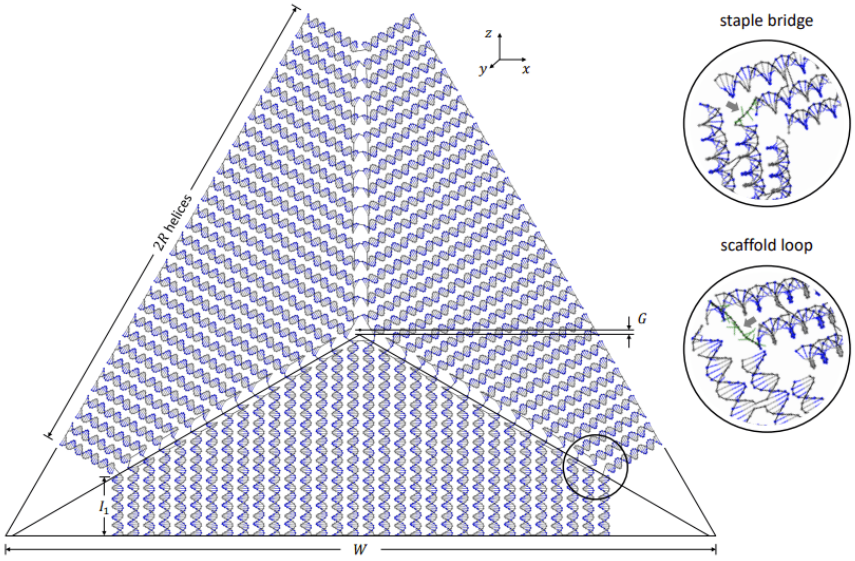

Figure 2.5: Adapted figure from Tikhomirov et al. [8] showing triangular tile design.

Chapter 3

Methods

3.1 DNA Origami Design and Synthesis

This section outlines the design, synthesis, and assembly process for three DNA origami structures utilized in this study: the 92x92 nm square tile, the 184x184 nm square tile, and the 270 nm hexagonal tile. Each subsection includes the computational design, assembly protocol, and purification steps.

Square Monomer Origami

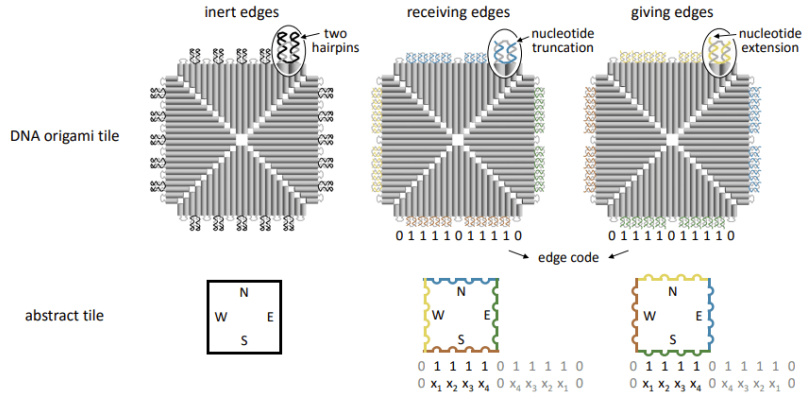

(a) Schematic of NESW designations and edge types. Adapted figure from Tikhomirov et. al. [7].

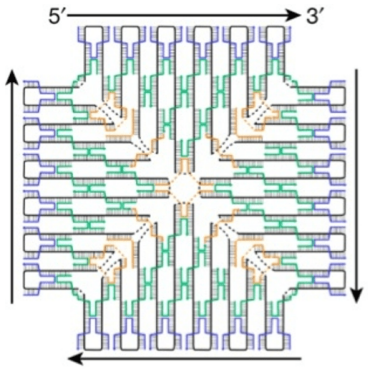

(b) Blueprint showing scaffold path and staple layout.

Figure 3.1: 92x92 nm DNA origami monomer tile.

Design and Computational Analysis

The square monomer tile is the fundamental building block for subsequent assemblies used in this work. The tile designed by Tikhomirov et al. [7] is folded from an M13mp18 scaffold strand (7,249 nt) and comprises 10 helices with 32 base pairs per helix, forming a square measuring 92x92 nm. The tile is oriented using cardinal directions (North, East, South, West), with each edge designed to "give" or "receive" through complementary sticky end sequences. This edge assignment enables controlled directional assembly and minimizes misalignment.

Synthesis and Assembly Protocol

- **Mixing:** Single-stranded M13mp18 scaffold strands (10 nM) are combined with a set of 206 staple strands (75 nM) in 1x TE buffer containing 12.5 mM $MgCl_2$.
- **Annealing:** The reaction mixture is initially heated to 90°C for 2 min, then gradually cooled to 20°C at 6 sec per 0.1°C.
- **Negation:** Following annealing, a five-fold excess of 44 negation strands is added to the mixture. The sample is subsequently cooled from 50°C to 20°C at 2 sec per 0.1°C.
- **Purification:** Assembled monomers are purified using Amicon Ultra-0.5 centrifugal filters (100 kDa MWCO) to remove excess staple strands and unbound scaffold DNA.

Square Tetramer Origami

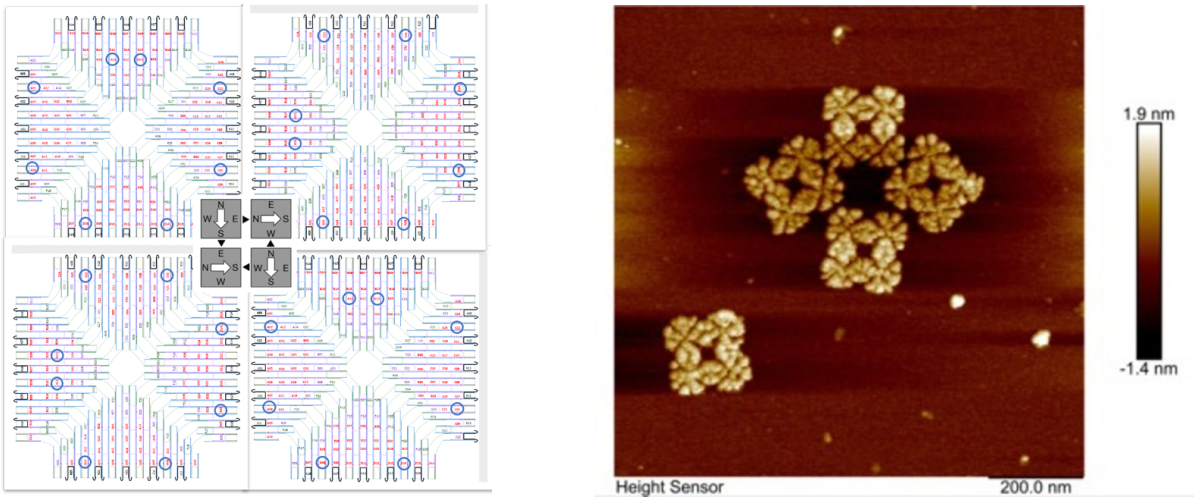

(a) Schematic of tile orientation and layout.

(b) AFM image of 2x2 square tiles.

Figure 3.2: 184x184 nm DNA origami tetramer tile.

Design and Computational Analysis

The tetramer structure is assembled from four 92 × 92 nm square monomers, following the design strategy introduced by Tikhomirov et al. [7]. Each monomer is connected through complementary edge sequences to form a 2×2 array measuring 184 × 184 nm. The NESW orientations facilitate controlled interactions at each edge. The assignment of "giving" and "receiving" edges enforces directional assembly.

Synthesis and Assembly Protocol

- **Mixing:** Monomers with their respective "giving" and "receiving" ends are mixed.
- **Annealing:** The reaction mixture is annealed from 55°C to 45°C at 2 min per 0.1°C and then from 45°C to 20°C at 6 sec per 0.1°C.
- **Purification:** The assembled tetramer is purified using the same ultrafiltration procedure as the monomer to remove excess DNA strands.

Hexagon Hexamer Origami

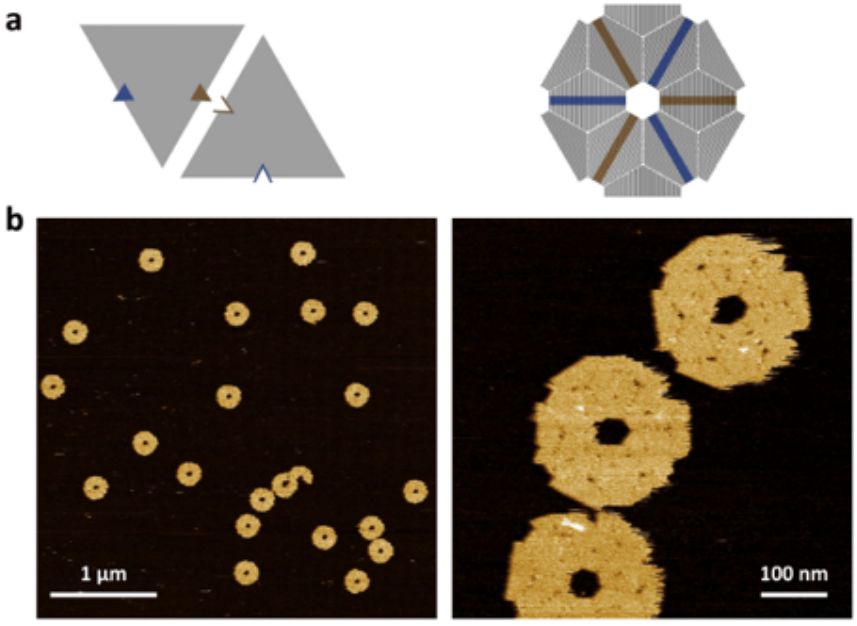

Figure 3.3: Schematic of hexagon tile construction. Adapted figure from Tikhomirov et. al. [8]. (a) Edge interactions that compose the assembled hexagon. (b) AFM images of 270 nm hexagon tiles.

Design and Computational Analysis

The hexagon tile is assembled from six triangular subunits, based on the design methodology outlined by Tikhomirov et al. [8]. Two distinct triangular tiles with designated giving and receiving edges guide specific hybridization, directing the formation of a hexagon with a diagonal of approximately 270 nm. The strategic arrangement of sticky end sequences ensures proper orientation, minimizing misalignments and promoting accurate assembly.

Synthesis and Assembly Protocol

- **Mixing:** Two separate tubes containing single-stranded M13mp18 scaffold strands (10 nM) are mixed with a set of 216 staple strands (15 nM) in 1x TE buffer with 12.5 mM $MgCl_2$. Each tube corresponds to one of the two distinct triangular tiles necessary for hexagon assembly.
- **Annealing:** The reaction mixtures are initially heated to 90°C for 2 minutes and then cooled to 20°C at a rate of 0.1°C per 6 seconds.
- **Negation:** Following the initial annealing, a ten-fold excess of 48 negation strands is added. The mixtures are then cooled from 50°C to 20°C at 2 sec per 0.1°C.
- **Purification:** The two tile mixtures are combined and then cooled from 50°C to 20°C at 2 min per 0.1°C.
- **Purification:** No purification step is performed following assembly.

3.2 Structural Verification and Yield Analysis

Following assembly, verifying the successful folding of desired DNA origami species is often necessary. This section outlines the verification methods employed within this work, along with the criteria for folding yield analysis. The protocols described here, developed in collaboration with the Ti Lab, incorporate modifications based on established practices in DNA nanotechnology.

Gel Electrophoresis

Agarose gel electrophoresis is employed to verify the assembly of DNA origami structures and confirm the presence of target species by comparing band intensities against a known DNA ladder. Gels were prepared using 0.5x TBE buffer with 12.5 mM $MgCl_2$ and stained with ethidium bromide (EtBr). Electrophoresis conditions were optimized based on structural complexity as follows:

- **Standard Structures (Monomers, 2x2 Arrays):** 1% (w/v) agarose gel, 75 V, 90 minutes.

- **Delicate Structures (Hexagons, 4x4 Arrays):** 0.6% (w/v) agarose gel, 45 V, 2 hours.

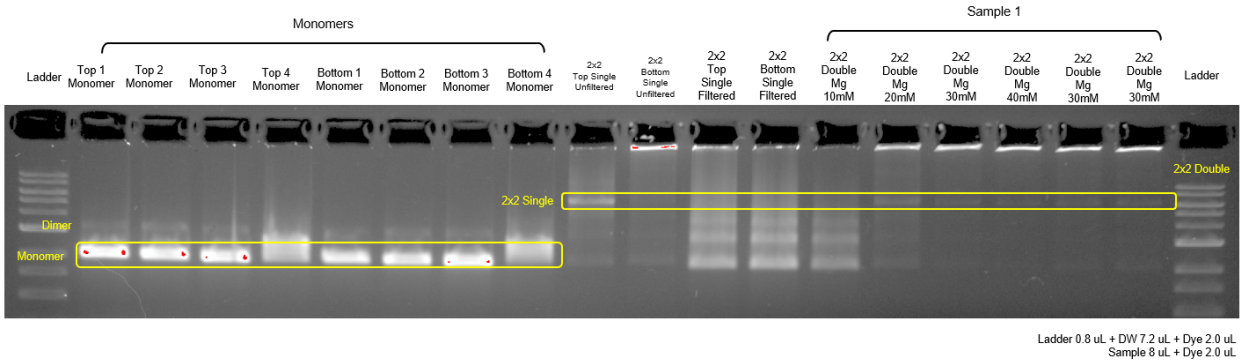

Figure 3.4: Example gel exhibiting strong monomer bands, verifying successful assembly.

AFM Measurement

Atomic Force Microscopy (AFM) is employed to verify the structural integrity of DNA origami assemblies and to assess the performance of placement techniques by evaluating both occupancy yield and binding quality to the substrate surface. AFM imaging is conducted using a Bruker AFM system with distinct modes, settings, and tip types, depending on the application. The specific AFM parameters for each mode are outlined in Table 3.1.

Table 3.1: AFM Imaging Parameters for Structure Verification and Placement Evaluation

Parameter	**Air Mode**	**Fluid Mode**
Experiment Type	ScanAsyst Air HR	ScanAsyst Fluid HR
Scan Tip	ScanAsyst Air HR	ScanAsyst Fluid
Scan Rate	3.82 Hz	3.03 Hz
Feedback Gain	4–6.2	3.42–22
PeakForce Setpoint	746 pN	460–820 pN
PeakForce Amplitude	100 nm	6 nm
Lift Height	64.8 nm	12 nm

The selection of specific AFM modes and parameters is determined by the experimental objective, as outlined below:

- **Structure Verification:** DNA samples are deposited on mica chips to verify correct assembly and quantify synthesis yield. This method is typically performed in fluid mode for optimal resolution, though air mode enables faster scanning.

- **Placement Evaluation:** DNA structures are imaged directly on silicon substrates to assess surface binding and distribution. Initially, scans were conducted in air mode. However, we later found that fluid mode imaged surface interaction more accurately, so the protocol was adjusted.

Folding Yield Analysis

Folding yield is determined by analyzing AFM images to quantify the number of correctly folded structures relative to unfolded or misfolded structures. The criteria for identifying fully folded structures are based on the method outlined by Kim [5], with emphasis on the following:

- Complete and consistent edge alignment.
- Absence of visible structural defects or truncations.
- Uniform morphology across multiple AFM images.

The folding yield (%) is calculated using the following formula:

$$\text{Yield (\%)} = \left(\frac{\text{Number of correctly folded structures}}{\text{Total number of structures}} \right) \times 100 \tag{3.1}$$

3.3 Mask Design for Surface Patterning

Three distinct masks were employed throughout this work, each serving a specific purpose in defining deposition areas for DNA origami placement using deep ultraviolet (DUV) lithography. The following subsections detail each mask's design, rationale, and key features.

Mask V1

- **Design:** Mask V1 is structured into three hierarchical layers to systematically assess deposition efficacy across varying pattern sizes and shapes:
  - Four main pattern regions, each consisting of left (circular patterns) and right (square patterns) patches.
  - Each patch is arranged as a 5x5 array of identical pattern blocks.
  - Within each block, a nested 5x5 array of patterns is structured into a 10x10 grid
  - Each of these 10x10 grids consists of patterns that range in size from 100 nm (top left) to 580 nm (bottom right)

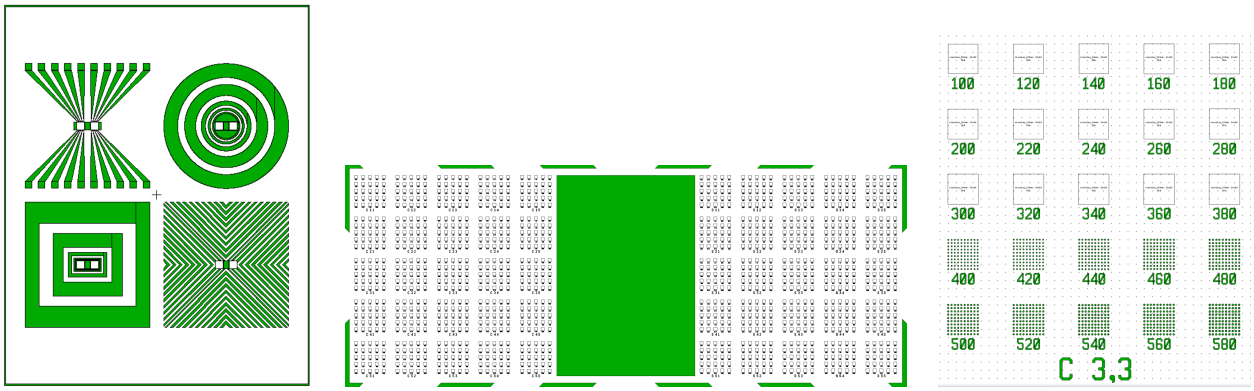

(a) Mask Overview. (b) Patterned Regions. (c) Nested Arrays.

Figure 3.5: Mask V1 is structured to evaluate DNA origami deposition across multiple pattern sizes and shapes without mask replacement. Figure shows the hierarchal layers of the mask.

- **Purpose:** This mask was the first one we tested and was designed to comprehensively evaluate deposition parameters without requiring multiple mask iterations. It enabled simultaneous testing of DNA origami of various sizes against a wide range of pattern dimensions to determine optimal deposition sizes and pattern-to-origami alignment.

Mask V2:

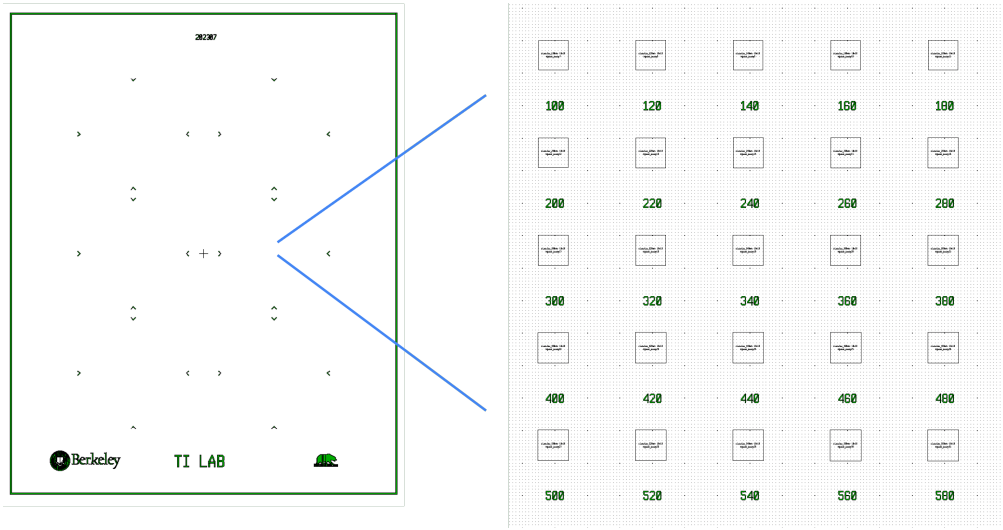

Figure 3.6: Mask V2 contains six 5x5 arrays of circular patterns with sizes ranging from 100 nm to 580 nm, allowing targeted assessment of deposition yield and origami alignment.

- **Design:** Mask V2 streamlines the testing structure by focusing on circular patterns and removing interfering regions:
  - The chip consists of six main pattern regions, each consisting of a 5x5 array.
  - Each 5x5 array consists of a nested 10x10 grid of circular patterns, with diameters ranging from 100 nm (top left) to 580 nm (bottom right).
  - The large hydrophilic PR regions in Mask V1 were removed to prevent nonspecific binding, ensuring that DNA origami targets the intended pattern sites.
- **Purpose:** Mask V2 refines the deposition testing strategy by eliminating variables associated with square patterns and hydrophilic PR regions. This allows for a more controlled evaluation of DNA origami alignment and yield across a range of circular pattern sizes.

Mask V3:

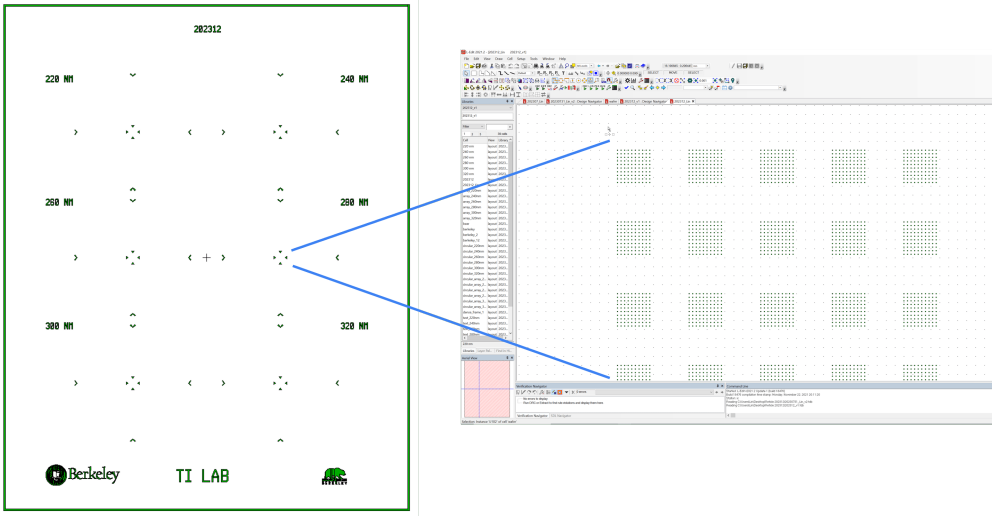

Figure 3.7: Mask V3 consists of six 5x5 arrays of circular patterns, each region containing uniform pattern sizes. Small PR arrow markers were added near the patterned regions to assist in locating specific areas during AFM imaging.

- **Design:** Mask V3 refines the pattern layout based on prior deposition results, focusing on sizes closely matching the hexagonal DNA origami dimensions:
  - Six main pattern regions, each consisting of a 5x5 array of circular patterns.
  - Each 5x5 array contains uniformly sized patterns, with sizes increasing across the six regions from 220 nm (top left) to 320 nm (bottom right).

  - Pattern size range was narrowed to align with the hexagonal DNA origami size.
  - Small PR arrow markers were added adjacent to each patterned region to aid in scribing and locating specific deposition sites during AFM imaging.

- **Purpose:** Mask V3 focuses on deposition parameters relevant to hexagonal DNA origami, with pattern sizes tailored to the target structure dimensions. Additionally, including PR markers facilitates the accurate localization of patterned areas during post-deposition AFM imaging.

3.4 Placement Techniques

This section outlines two distinct binding strategies for DNA origami placement: magnesium ion-facilitated bridging and aptamer-based binding. Each method employs a different surface preparation and functionalization approach to achieve controlled placement of DNA nanostructures onto Si/SiO_2 substrates.

Oligo-Facilitated Binding via GPTMS Functionalization

Oligo-facilitated binding utilizes GPTMS functionalization to covalently anchor DNA aptamers onto the substrate surface, allowing for sequence-specific hybridization of DNA origami structures. The GPTMS functionalization workflow was developed to facilitate site-specific DNA origami placement using amine-terminated oligonucleotides. The complete workflow is shown in Figure 3.8 and is outlined as follows:

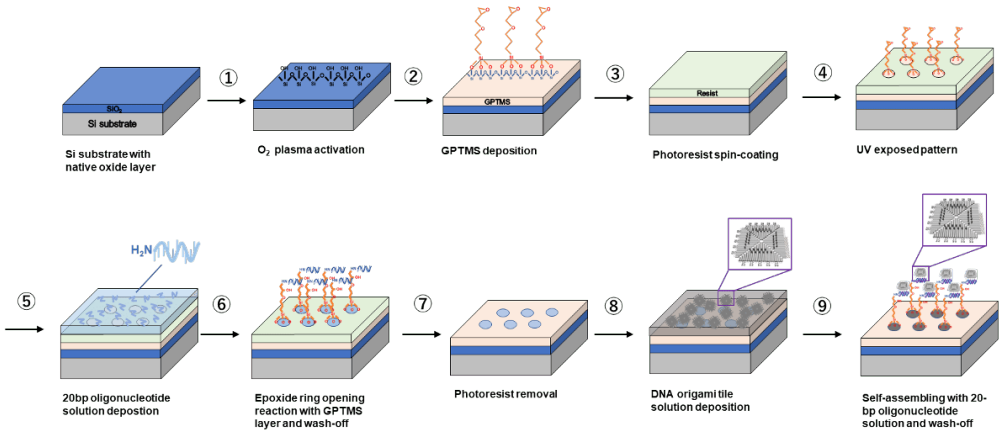

Figure 3.8: Workflow for GPTMS functionalization and DNA origami deposition.

1. **Substrate Preparation:** Obtain silicon substrates with a 100 nm silicon oxide layer (6" wafer). Sonicate in acetone for 2 min. Sonicate in IPA for 2 min.

2. **Surface Activation:** Treat the substrate with O_2 plasma using Ptherm system at 100 W, 100 sccm, for 10 min.

3. **GPTMS Functionalization:** Immerse the substrate in a 2% (v/v) GPTMS solution in toluene for 20 hr. Rinse thoroughly in toluene with sonication for 10 sec. to remove unbound or agglomerated silane.

4. **Photoresist Application:** Spin coat UV210 photoresist to a thickness of 290 nm. Bake at 130°C for 90 sec. Expose the wafer using ASML300 at 30 mJ/cm^2. Post exposure bake and develop with MF26A.

5. **Scribing and Chip Definition:** Use a wafer scriber to cut the wafer into individual chips. Scribe on each chip to define the deposition area, ensuring that each region is clearly marked for AFM imaging. Clean each chip with an air gun.

6. **Oligonucleotide Deposition:** Apply 20 μL of 5 μM 20-bp oligonucleotides in 50 mM sodium phosphate buffer to the patterned regions. Incubate for 5 min. and then heat in an oven at 75°C for 1 hr. Briefly submerge the wafer in 0.4% SDS (sodium dodecyl sulfate) solution for 1 min., followed by a DI water rinse to remove excess DNA.

7. **Photoresist Removal:** Sonicate in acetone for 2 min. Sonicate in IPA for 2 min. Dry the wafer with N_2.

8. **BSA passivation:** Deposit 200 μL of BSA (bovine serum albumin) in 1X PBS on pattern area. Incubate for 1 hr. and then dry with N_2.

9. **Origami Deposition:** Apply 20 μL of DNA origami solution onto the substrate. Incubate under specified parameters. Rinse by immersing in DI water for 30 sec. twice. Use an air gun to dry the substrate thoroughly.

Workflow Modifications

Initial testing revealed issues with overexposure and incomplete wash-off. The following modifications were implemented:

1. **Photoresist Development:** UV exposure reduced from 32 to 30 mJ/cm^2.

2. **BSA passivation:** BSA immersion was added before origami deposition to prevent excessive background binding, further detailed in 4.3.

Binding Mechanism

The GPTMS surface was functionalized using amine-terminated oligonucleotides that reacted with the epoxy groups via nucleophilic ring-opening reactions. The tested oligonucleotide

Table 3.2: Oligonucleotide Sequences Tested for Surface Functionalization

Oligo #	Description	Sequence
1	5Cy5-oligo-amine	/5Cy5/GG AGA GAA GAG GGA AGG AAA /3AmMO/
2	oligo-amine	GG AGA GAA GAG GGA AGG AAA /3AmMO/
3	amine-oligo	/5AmMO/GG AGA GAA GAG GGA AGG AAA
4	8bp oligo-amine1	GGA GAG AA /3AmMO/
5	amine-8bp oligo	/5AmMC6/GG AGA GAA
6	amine-8bp T	/5AmMC6/TT TTT TTT

sequences, listed in Table 3.2, included a range of amine-terminated, Cy5-labeled, and short oligos to assess binding efficacy and surface coverage.

The epoxy-amine reaction facilitates the covalent attachment of amine-terminated oligonucleotides to the epoxy groups on the GPTMS-modified surface, effectively anchoring the oligos to the substrate. This surface functionalization enables the subsequent binding of DNA origami structures to the surface-bound oligonucleotides in distinct orientations, as illustrated in Figure 3.9. By adjusting the orientation of the complementary strands on the origami, the binding mode can be modulated to favor either (a) a vertical, stilt-like configuration where a gap is left between the origami and the substrate or (b) a horizontal, zipper-like configuration where the origami lies closer to the surface through multiple lateral connections.

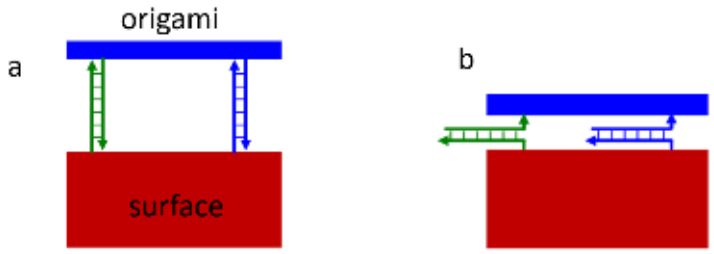

Figure 3.9: Potential binding modes of DNA origami to surface-bound oligonucleotides. (a) Vertical, stilt-like binding. (b) Horizontal, zipper-like binding.

Electrostatic Binding via Magnesium Ion Bridging

Magnesium ion bridging leverages electrostatic interactions to facilitate the site-specific deposition of DNA origami onto pre-patterned substrates. This method employs Mg^{2+} ions to mediate binding between negatively charged DNA structures and positively charged sur-

face domains, enabling controlled placement without covalent modifications. The complete workflow is shown in Figure 3.10 and is outlined as follows:

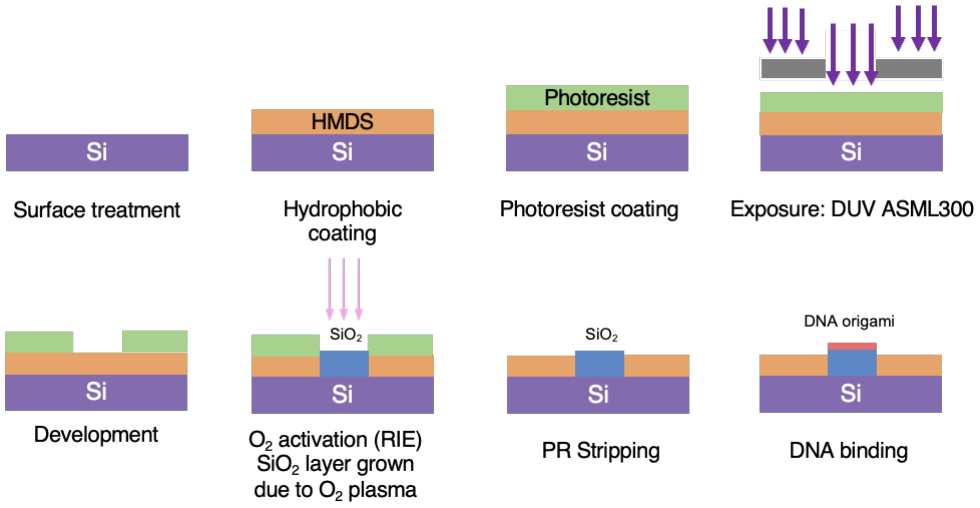

Figure 3.10: Workflow of Magnesium Ion Bridge Deposition and DNA origami placement.

- **Substrate Preparation:** Obtain silicon substrates with a native silicon oxide layer (6" wafer, prime grade, low roughness 0.2 nm). Sonicate in IPA for 2 min. Dry with N_2.
- **Surface Activation:** Clean with O_2 plasma using ptherm (Plasma-Thermal Parallel Plate Plasma Etcher) system at 100 sccm, 90 mTorr, 100 W for 10 min to generate surface silanols.
- **HMDS (Hexamethyldisilazane) Coating:** Bake the substrate on a hot plate at 150°C for 30 min to dehydrate the surface. Place the substrate in a 4 L chamber saturated with HMDS vapor for 30 min to introduce trimethyl silyl groups. Bake the substrate again at 150°C for 30 min to stabilize the silanized surface.
- **Photoresist Application and Patterning:** Spin coat UV210 photoresist to a thickness of 280 nm. (Spin coating with 3630 rpm, soft baking 140°C, 90 sec). Bake at 130°C for 90 sec. Expose the wafer using ASML300 at 48 mJ/cm^2. Post-exposure bake (PEB, 110°C for 60 sec) and develop with MF26A for 60 sec puddle and repeat without PEB for 3 times.
- **Scribing and Chip Definition:** Use a wafer scriber to cut the wafer into individual chips. Scribe on each chip to define the deposition area, ensuring that each region is clearly marked for AFM imaging. Clean each chip with an air gun.

- **Chip Activation:** Activate the binding site of the chip with short anisotropic O_2 etch with RIE at 80 mTorr, 80 sccm, 80 W for 30 sec.
- **Photoresist Removal:** Sonicate in 1165 photoresist removal for 5 min twice to strip remaining photoresist. Sonicate in IPA for 5 min to remove any residue.
- **Origami Deposition:** Apply 20 μL of DNA origami solution onto the patterned region. Incubate under specified parameters and placement buffer (5 mM Tris, pH 8.35, Mg^2+ varied).
- **Washing:**
  - Initial washing: 8 rinses with placement buffer, 60 μL per rinse.
  - Tween washing: 5 rinses with 0.1% Tween 20 in placement buffer, 20 μL per rinse.
  - Final washing: 8 rinses with placement buffer adjusted to pH 8.9, 60 μL per rinse.

Workflow Modifications

Following initial testing, inconsistencies in DNA origami binding and placement prompted the following modifications to the workflow:

1. **Photoresist Development:** The development dose was increased from 32 to 48 mJ/cm^2 to optimize pattern dimensions in the 260–270 nm range, ensuring consistent feature sizes for targeted DNA origami alignment.
2. **Magnesium Reduction:** The Mg^{2+} concentration was reduced from Gopinath et. al.'s original protocol to prevent origami structural deformation and maintain integrity during incubation.
3. **Drying Step Removal:** The drying step following washing was removed to prevent interference with binding.

Binding Mechanism

Magnesium ions (Mg^{2+}) are electrostatic bridges, facilitating non-covalent interactions between the negatively charged DNA origami and the negatively charged surface domains. Despite DNA and the substrate carrying net negative charges, Mg^{2+} ions can act as mediators, forming ionic linkages that stabilize the DNA origami on the surface. The binding mechanism is illustrated in Figure 3.11.

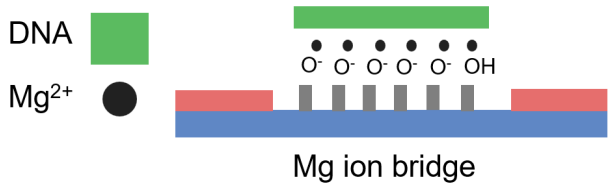

Figure 3.11: Mechanism of electrostatic DNA origami binding via Mg^2+ ion bridging.

Chapter 4

Experiments and Results

4.1 DNA Design and Yield Optimization

This section describes various modifications to the synthesis process and design of DNA origami implemented in response to challenges observed during the optimization of the magnesium ion bridge placement method.

Double-Layer 2x2 Origami Synthesis

While exploring anti-folding measures for origami, we proposed a double-layer 2x2 tile design. This approach aimed to enhance the rigidity of the origami and provided additional structural stability, notably since the single-layer 2x2 tiles exhibited undesired deformation.

The double-layer design involved a connector strategy, wherein specific staple strands were extended to form bridging elements between the two layers. These connectors were intended to anchor the two layers while maintaining the intended spatial alignment. We suggested several variations of these connectors, ranging from single-strand crossovers to more complex multi-strand junctions. Figure 4.1 depicts the proposed connector designs.

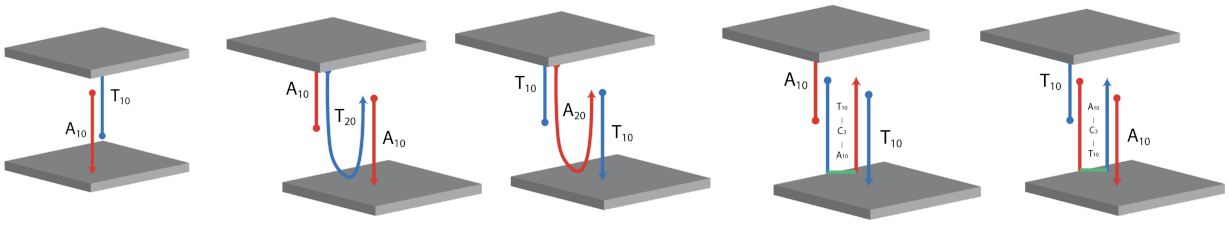

Figure 4.1: Proposed connector variations for double-layer synthesis.

The proposed protocol for double-layer 2x2 origami synthesis follows the single-layer 2x2 origami synthesis and includes the following steps:

- **Mixing:** 500 pM of each 2x2 tile (top and bottom) with the appropriate extension strands and the specified connector strand (16 nM in 1xTE) are mixed in a 30 mM $MgCl_2$ buffer.
- **Annealing:** The reaction mixture is annealed from 40°C to 20°C at 12 min per 0.1°C.
- **Purification:** The assembled structure is purified using the same ultrafiltration procedure as the monomer to remove excess DNA strands.

After establishing the connector designs, we proceeded with synthesizing double-layer 2x2 origami tiles. However, initial attempts revealed challenges in achieving robust folding and high yield. To systematically assess these issues, we employed gel electrophoresis to analyze the composition of synthesized structures at various stages of the annealing process.

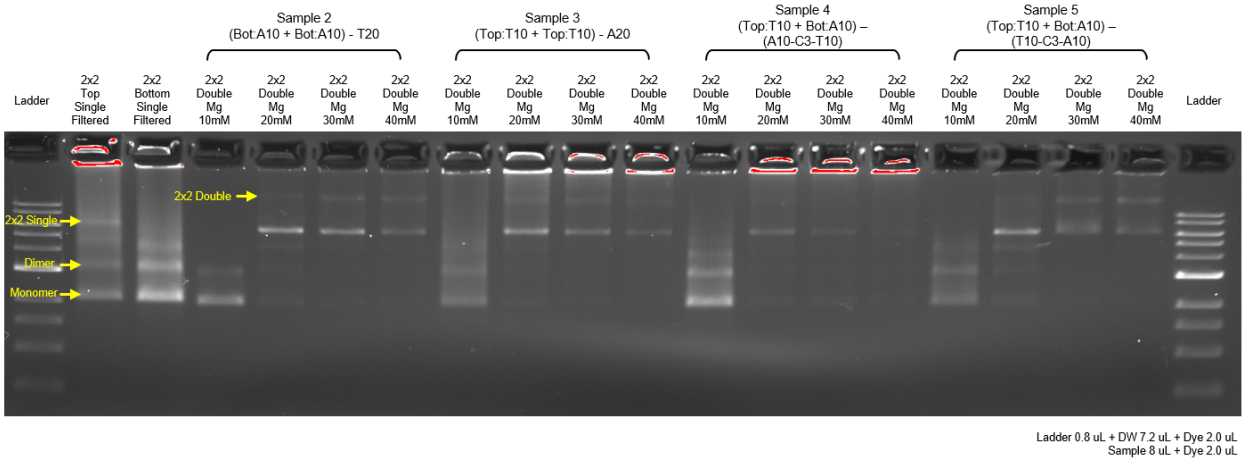

Figure 4.2: Gel electrophoresis analysis of a synthesis experiment. Absence of distinct bands corresponding to single-layer and double-layer 2x2 tiles indicates poor yield.

The gel electrophoresis data (Figure 4.2) revealed a lack of the expected bands corresponding to single-layer and double-layer tiles. This outcome indicated that the yield of 2x2 tiles was bottlenecking downstream attempts to create double-layer structures.

To further verify these findings, we employed AFM imaging to visualize the synthesized structures. While we found some double-layer tiles, they were sparse and inconsistently distributed, as shown in Figure 4.3.

We identified critical errors in the origami synthesis protocol through these diagnostic steps. Specifically, inaccuracies in pipetting small volumes led to inhomogeneous mixtures, resulting in stochastic variations that diminished overall yield. This issue was critical as precise strand ratios are crucial for consistent folding in any tile.

Although we did not pursue optimization of the double-layer synthesis protocol further because other solutions resolved the folding issues, the insights gained from these investigations informed subsequent synthesis attempts and improved overall synthesis yield.

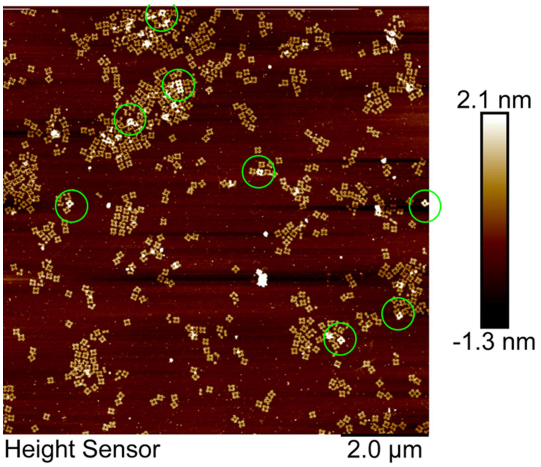

(a) Sparsely distributed double-layer tiles.

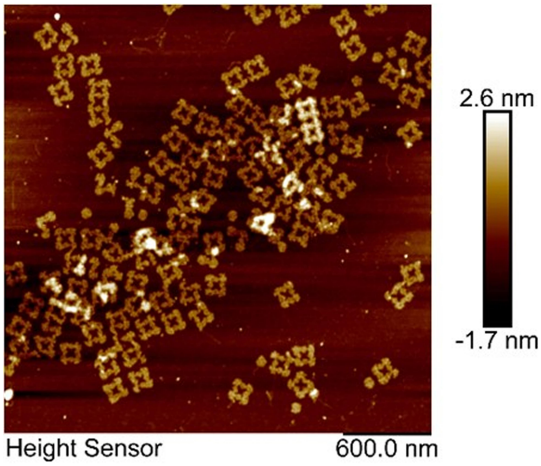

(b) Closer view of brighter, taller 2x2 tiles.

Figure 4.3: AFM images of double-layer synthesis. Double-layer tiles are identifiable by their brighter, taller profiles but are present in low concentrations, indicating poor yield.

Strong Hexagon Origami Synthesis

We developed a modified hexagonal tile responding to structural instability observed in varying buffer conditions. This design increased the length of the edge extensions that connect adjacent tiles from 2 nt to 8 nt, thereby enhancing inter-tile connections.

Following this modification, we also observed a significant improvement in base synthesis yield, increasing from 75% in the original hexagonal design to 90% in the Strong Hex (Figure 4.4). AFM imaging further confirmed the structural robustness of the Strong Hex, revealing more uniform tiles that maintained their structure across changing buffer conditions.

The structural enhancement provided by the 8 nt extensions was particularly effective in preventing premature disassembly of hexagonal tiles during deposition, underscoring the importance of edge extension length in stabilizing multi-tile assemblies.

Hexagon Modifications for Anti-Stacking and Aggregation

We further modified the hexagon tile design to address persistent issues with tile aggregation and stacking during deposition. Specifically, we introduced polyC14 extensions along the edges of each hexagon tile, aiming to increase the spatial separation between adjacent tiles and reduce the likelihood of lateral aggregation.

In parallel, polyT20 extensions were incorporated onto the upward-facing surface of each hexagon tile in a cyclonal orientation. These extensions served dual purposes: (1) acting

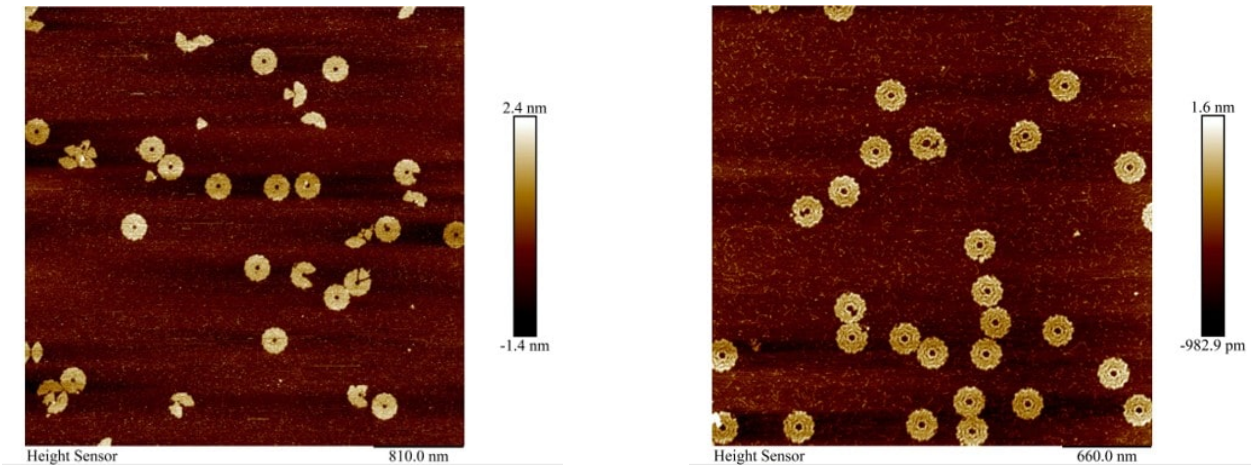

(a) Normal Hex (b) Strong Hex

Figure 4.4: Comparison of hexagonal tile stability and yield. (a) Normal Hex exhibits lower yield and structural integrity. (b) Strong Hex demonstrates higher yield and robustness.

as structural elements to reduce vertical stacking by disrupting face-to-face contact between tiles, and (2) as AFM imaging markers, appearing as brighter, more distinct features under AFM due to their increased length and orientation.

Despite these adjustments, some degree of vertical aggregation persisted, indicating that further refinements to extension length and orientation may be necessary to fully eliminate inter-tile interactions under deposition conditions.

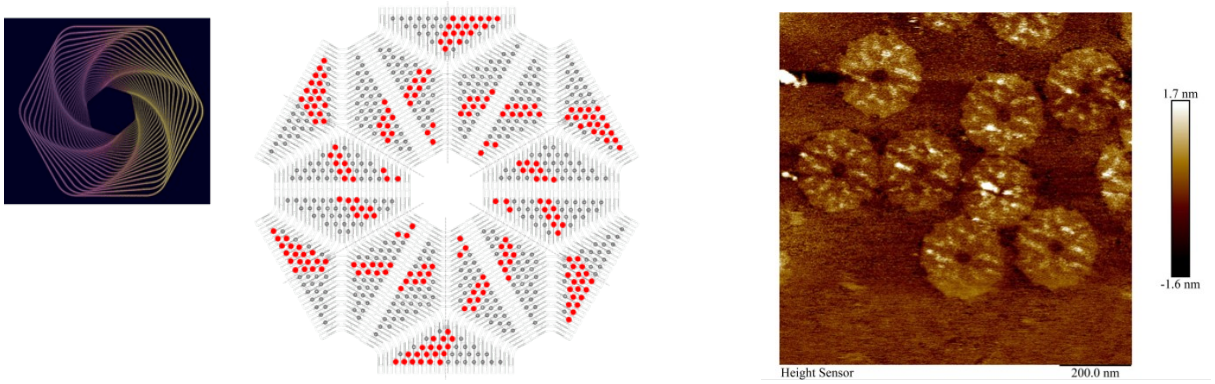

(a) Cyclonal hex with polyC14 / polyT20 extensions. (b) AFM close-up of extensions.

Figure 4.5: Optimized hexagon design incorporating polyC14 and polyT20 extensions to mitigate stacking and aggregation.

Introducing polyC14 and polyT20 extensions decently reduced lateral aggregation and

provided clearer AFM imaging markers. However, further optimization is necessary to prevent vertical stacking and unintended inter-tile interactions.

4.2 Lithography and Substrate Optimization

In optimizing lithography and substrate for electrostatic binding, we approached the process through two main strategies: reducing wafer roughness and tuning the PR exposure dosage. Both were pivotal steps aimed at mitigating origami folding and aggregation observed during the initial experiments on GPTMS functionalization.

Surface Flattening for Origami Deposition

Initial deposition experiments using thermally grown SiO_2 layers treated with HMDS revealed that the surface roughness was relatively high (∼1 nm), comparable to the thickness of DNA origami structures (∼1 nm). We hypothesized that this roughness was a major contributor to the unintended folding observed during deposition, as contact with the surface could form bends and encourage the origami to fold in on itself.

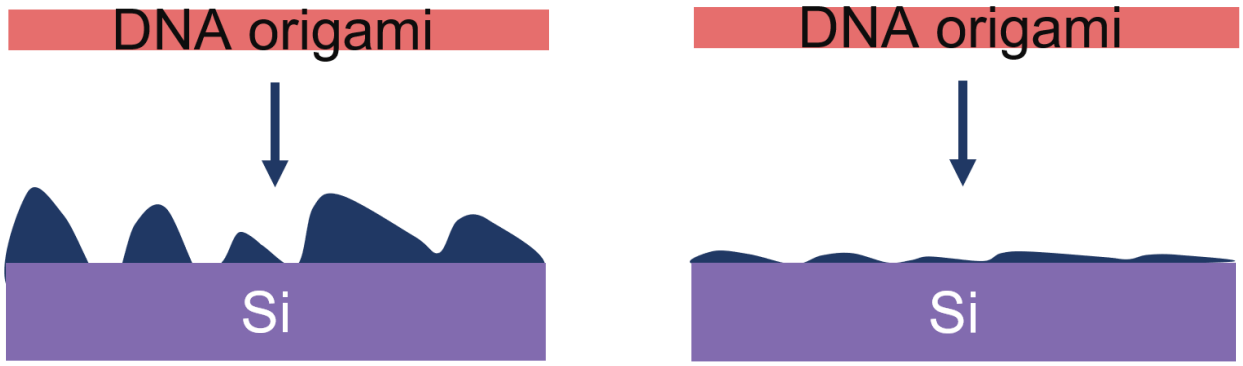

(a) High surface roughness.

(b) Low surface roughness.

Figure 4.6: Hypothesized model of surface roughness. (a) High roughness could encourage origami folding. (b) Smoother surface minimizes unwanted folding interactions.

To address this, we transitioned to a chemical oxide layer formed on native Si wafers. The process involved a hydrogen fluoride (HF) treatment to strip the native oxide, followed by controlled oxidation to create a new, smoother oxide layer. This treatment effectively reduced the surface roughness from 1.0 nm (10 angstroms) to approximately 0.17 nm (1.7 angstroms). AFM analysis (Figure 4.7) confirmed the reduction in surface roughness, with the chemically grown oxide layer exhibiting substantially more uniform topography.

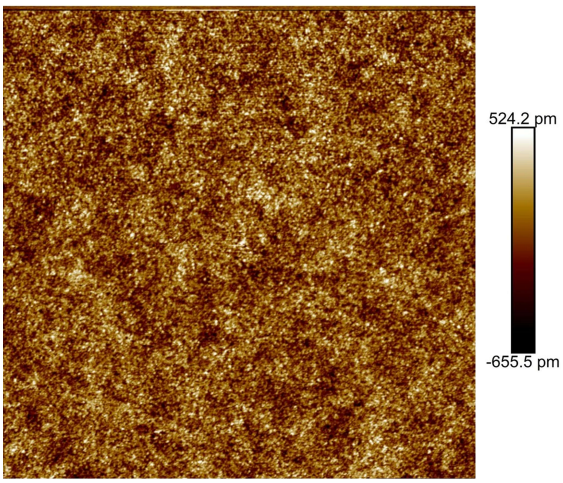

(a) Thermally grown SiO_2 layer.

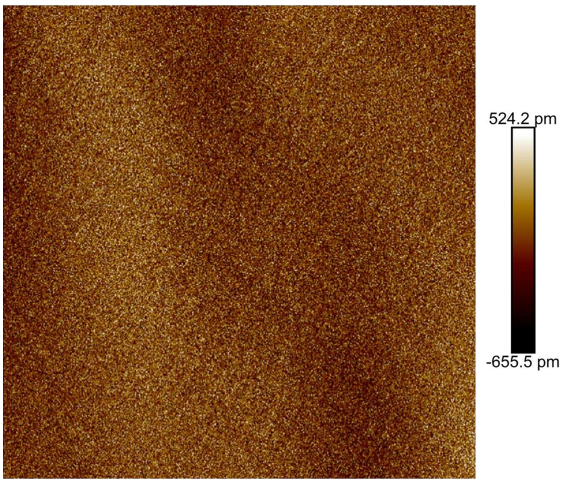

(b) Chemical oxide layer formation.

Figure 4.7: AFM comparison of surface roughness. (a) Thermally grown layer exhibits roughness of 10 angstroms. (b) Chemical oxide layer achieves roughness of 1.7 angstroms.

By reducing the surface roughness, the chemical oxide layer provided a more controlled deposition environment for DNA origami structures, significantly reducing unintended folding. This modification proved crucial for maintaining tile integrity during deposition.

PR Exposure Tuning for Pattern Size Optimization

Another optimization focused on refining the pattern dimensions through precise photoresist (PR) exposure dosage control. During initial experiments, the feature sizes of the patterned areas were inconsistent with the dimensions of the DNA origami tiles, allowing multiple tiles to occupy and interact with a single site, resulting in increased aggregation and stacking.

To address this, we systematically explored PR exposure dosages to align the feature size more closely with the intended dimensions of the hexagonal DNA origami. Exposure doses ranging from 30 to 60 mJ/cm^2 were tested, with six dosages shown in Figure 4.8. SEM imaging was employed to measure the resulting feature sizes.

The determined optimal PR exposure dosage was **48 mJ/cm^2**, as it produced pattern sizes most closely aligned with the hexagon tile dimensions of 270 nm. Additionally, plasma processing parameters were refined to 50 sccm at 80-90 mTorr for 30 seconds to enhance pattern fidelity.

This approach effectively reduced aggregation and stacking within patterned areas and minimized the likelihood of multiple origami interacting with a single site, thus enhancing overall placement fidelity.

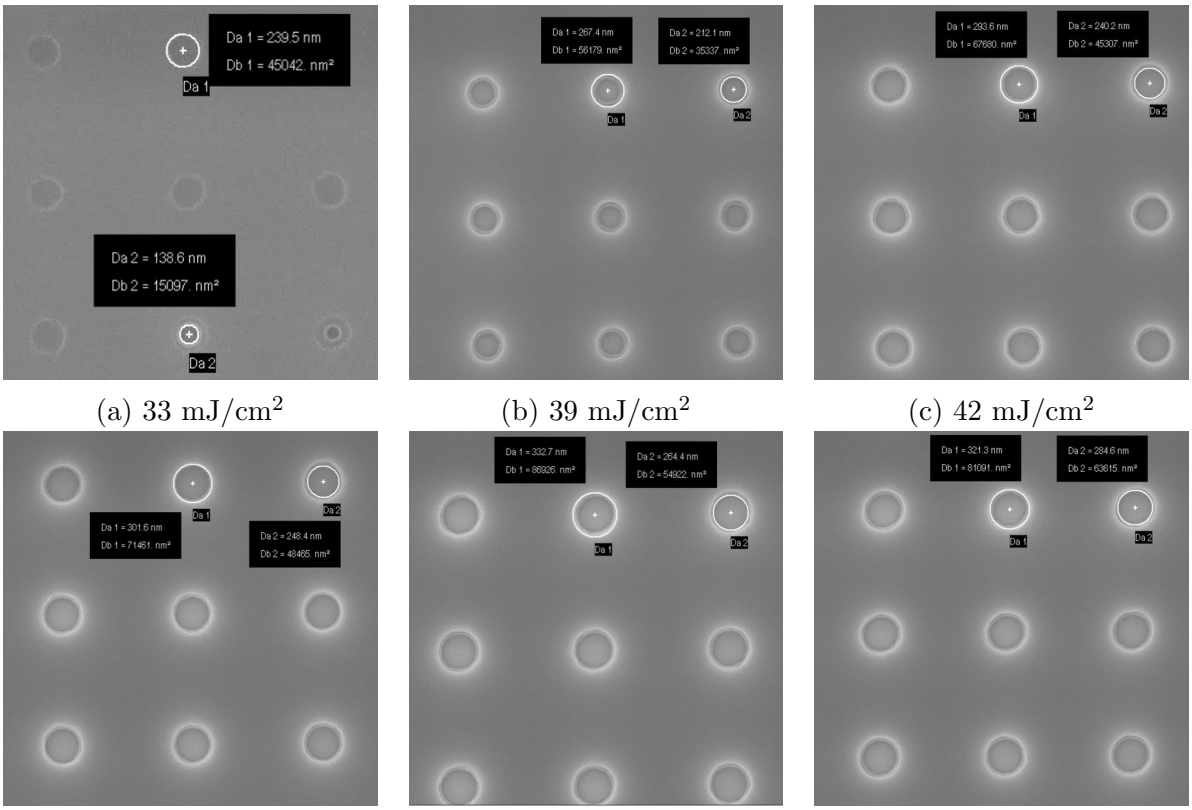

(a) 33 mJ/cm^2 (b) 39 mJ/cm^2 (c) 42 mJ/cm^2

(d) 45 mJ/cm^2 (e) 48 mJ/cm^2 (f) 54 mJ/cm^2

Figure 4.8: SEM images showing the effect of PR exposure dosage on feature size.

4.3 Oligo-Facilitated Binding via GPTMS Functionalization

Background Binding Mitigation and Surface Passivation

In the early stages of this work, significant background binding of DNA origami was observed on the substrate surface. Although the methodology was adapted from Gopinath et al.'s approach [2], the use of UV210 did not effectively passivate the GPTMS and SiO_2 layers, resulting in substantial nonspecific binding. Incorporating an HMDS layer slightly reduced nonspecific interactions but did not achieve sufficient hydrophobicity to eliminate background binding.

To address this issue, a BSA (Bovine Serum Albumin) passivation step was introduced before DNA origami deposition, as noted in 3.4. BSA is a protein that readily adsorbs to surfaces, forming a dense, hydrated layer that effectively blocks potential binding sites. This layer creates a protective barrier that prevents DNA origami from interacting with

the underlying surface, significantly reducing background binding by 99%. Meanwhile, the oligonucleotide-modified GPTMS regions remain accessible for specific hybridization, maintaining spatial control while minimizing unwanted binding.

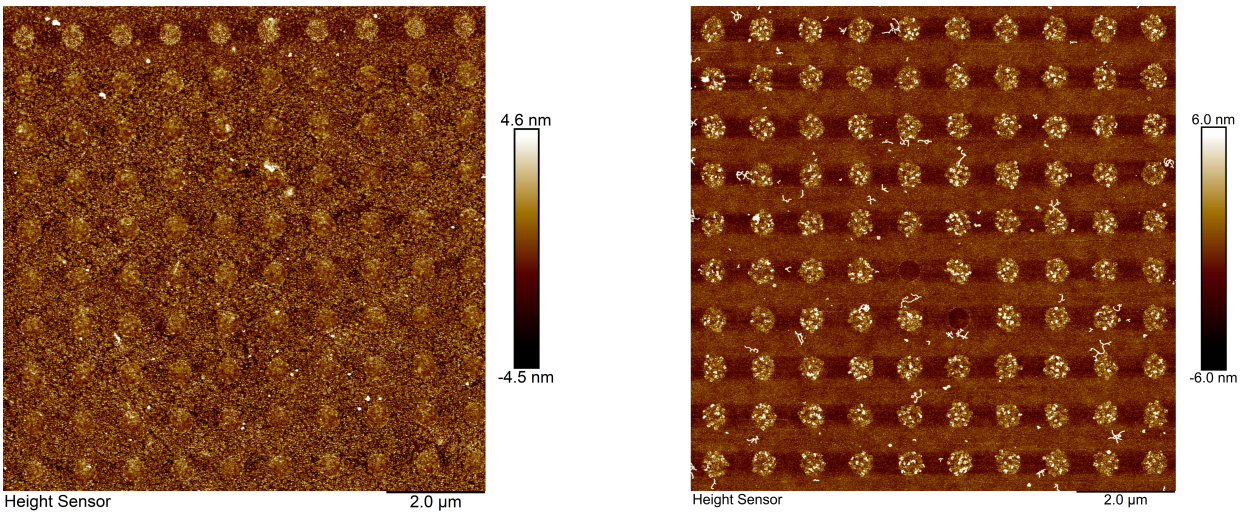

(a) Before BSA Treatment

(b) After BSA Treatment

Figure 4.9: Comparison of surface binding before and after BSA treatment. (a) Without BSA application, DNA origami nonspecifically adheres to the background. (b) With BSA application, nonspecific binding is significantly reduced, improving binding specificity.

Additionally, our collaborators, Ricardo Ruiz and Beifang Yu, explored an alternative surface modification strategy utilizing PMMA-OH brush layers to improve passivation and mitigate nonspecific binding more effectively than HMDS, as shown in Figure 4.10 [9]. The PMMA-OH brush layer forms a thin, polypeptoid monolayer on the surface that exhibits minimal binding affinity towards DNA origami, effectively blocking nonspecific binding sites. Unlike HMDS, which creates a hydrophobic, trimethylsilyl-terminated surface, the PMMA-OH layer offers a more tunable and versatile platform for surface passivation. Figure 4.11a illustrates the effect of the PMMA-OH layer in reducing nonspecific binding of DNA origami outside of patterned regions, showing comparable performance to BSA treatment.

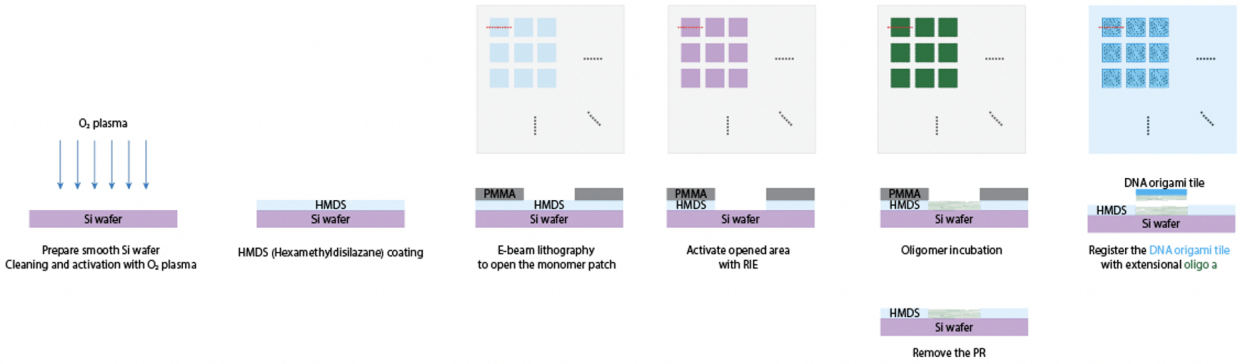

Figure 4.10: Workflow for PMMA-OH brush and DNA origami placement.

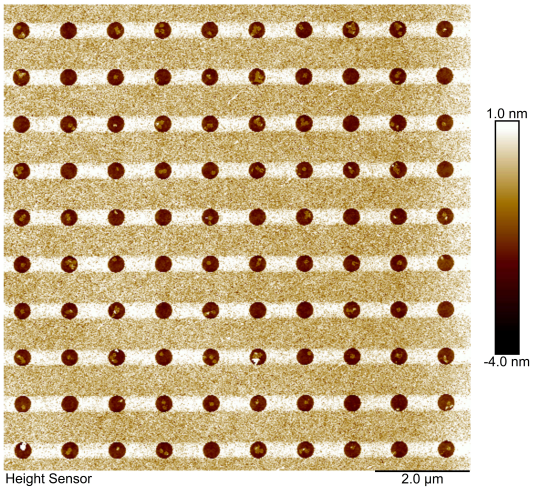

(a) 10x10 pattern of DNA origami deposition.

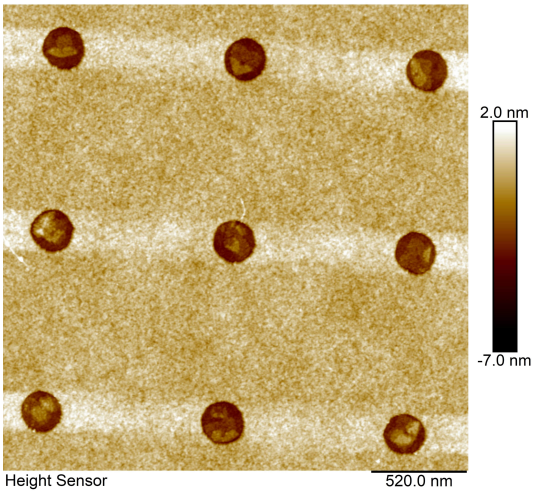

(b) Zoomed-in 3x3 region on same surface.

Figure 4.11: DNA origami deposition on PMMA-OH treated surfaces. (a) Reduced background binding is observed. (b) Smaller region reveals folding of origami within patterns.

Buffer and Deposition Parameter Testing

Before implementing BSA passivation, several buffer and deposition parameters were systematically tested to assess their impact on oligonucleotide binding and background reduction. These parameters included variations in oligo type, DNA origami concentration, magnesium chloride and sodium chloride concentrations, incubation time, temperature, and agitation (shaker presence). The tested combinations are summarized in Table 4.1.

Table 4.1: Tested Parameters for GPTMS Functionalization and Oligo Deposition

Oligo Type	Origami (nM)	$MgCl_2$ (mM)	NaCl (mM)	Time (min)	Temp (°C)	Shaker
1	1	12.5	0	30	Room	No
1	1	2	0	30	Room	No
1	1	2	0	30	Room	Yes
1	1	2	0	30	45	No
1	1	2	0	30	Room	No
1	1	5	0	30	Room	No
1	1	5	0	30	Room	No
1	1	5	0	30	Room	No
1	10	10	0	30	Room	No
1	10	10	0	30	Room	No
1	10	10	0	30	45	Yes
1	10	10	100	30	Room	No
1	10	12.5	0	30	Room	No
1	10	6	0	30	Room	No
1	10	8	0	30	Room	No
1	3	10	100	30	Room	No
1	5	10	0	30	Room	No
1	5	10	0	30	50	No
1	5	10	0	30	75	No
1	5	10	100	30	Room	No
1	5	2	0	30	Room	No
1	5	5	0	30	Room	No
1	5	8	0	30	Room	No
1	7.8	5	0	30	Room	No
2	10	10	0	30	Room	No
2	10	10	100	30	Room	No
3	10	10	0	30	Room	No
3	10	10	100	30	Room	No
3	3	10	100	30	Room	No
3	5	10	0	30	Room	No
3	5	10	0	30	50	No
3	5	10	0	30	75	No
3	5	10	100	30	Room	No
3	5	10	100	30	40	No
3	5	10	100	30	50	No
3	5	20	100	30	Room	No
3	5	20	100	30	40	No
3	5	20	100	30	50	No
3	7.8	5	0	30	Room	No
4	3	10	100	30	Room	No
5	3	10	100	30	Room	No
6	3	20	100	30	Room	No

Despite exploring various parameters, no significant reduction in background binding was observed, leading to the decision to implement BSA as a passivation layer and introduce hydrophobic surface treatments.

Folding and Aggregation Issues

Although successful reduction of background binding was achieved through both BSA and PMMA-OH treatment, DNA origami folding within the GPTMS-patterned areas persisted, as shown in Figure 4.11b. This suggests that further optimization of oligonucleotide orientation, density, and surface chemistry is necessary to mitigate folding and enhance placement precision. While our collaborators continued to refine this PMMA-OH-based strategy, this work primarily focused on the electrostatic magnesium ion bridge method.

Nevertheless, the GPTMS functionalization approach provided valuable insights into oligonucleotide-mediated placement, offering high spatial control and addressability and potentially stronger, more irreversible binding than Mg^{2+} ion bridging. Despite its more complex fabrication process and higher costs due to oligonucleotide synthesis and deposition, it remains a promising approach, with ongoing efforts by our collaborators. Given its precise spatial control, we expect this method to hold particular potential for applications where the orientation of the origami is critical, enabling controlled alignment of origami structures within patterned areas. Future work may involve optimizing the oligonucleotide sequence length, density, and spatial arrangement to mitigate folding while maintaining binding specificity and spatial precision.

4.4 Electrostatic Binding via Magnesium Ion Bridging

The ion bridge placement strategy employed in this study largely follows the methodology outlined by Gopinath et al., which utilizes magnesium ions as a bridging agent to mediate the electrostatic attachment of DNA origami to lithographically defined binding sites on silicon substrates [2]. Various folding and placement buffer conditions were explored to assess the effects on origami placement yield and fidelity.

Monomer Placement Verification

We initially reproduced Gopinath et. al.'s experimental setup to verify the efficacy of Mg^{2+} bridging under photolithographic conditions [2]. Initial results confirmed successful monomer placement with relatively high single-occupancy yield.

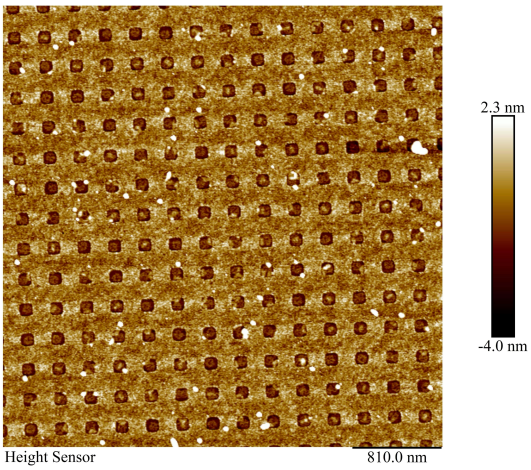

(a) 10x10 region monomer DNA deposition.

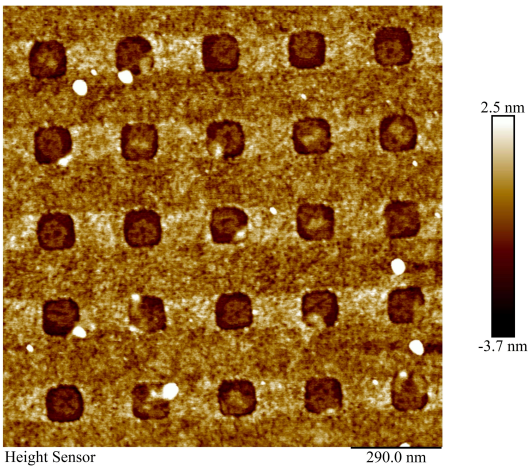

(b) Zoomed-in 4x4 region of same surfaace.

Figure 4.12: AFM images of PMMA-OH treated chip deposited with monomer origami.

Folding Mitigation

The GPTMS experiments highlighted significant folding issues for multi-tile (2x2) origami structures, suggesting that surface roughness and magnesium concentration may contribute to structural deformation.

Origami Structural Integrity and Rigidity

To counteract potential folding due to excessive electrostatic interactions, we proposed a double-layered 2x2 origami tile design to increase structural rigidity. However, initial synthesis experiments yielded suboptimal results due to low assembly yield, as detailed in Section 4.1.

Surface Roughness Reduction

In parallel, the substrate preparation protocol was adjusted to minimize surface roughness and the presence of high-angle surface features that could induce DNA origami folding. The refined lithographic process, detailed in Section 4.2, effectively produces a smoother wafer surface. This modification significantly reduced origami folding under controlled, lower Mg^{2+} concentrations (Figure 4.13).

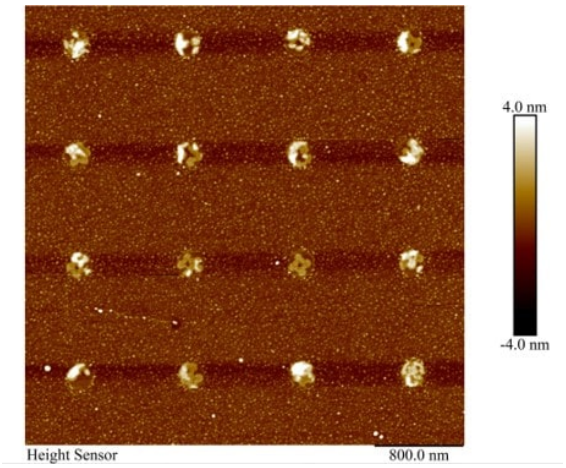

(a) 4x4 region of HMDS treated surface.

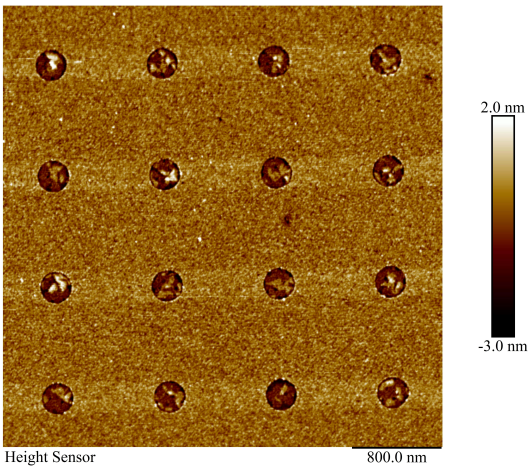

(b) 4x4 region of PMMA-OH treated surface.

Figure 4.13: AFM images of deposition on smoothed surfaces. The binding sites can be observed to be generally more uniform in height, indicating flatter, unfolded origami.

Aggregation and Stacking Mitigation

Following folding mitigation, persistent aggregation and stacking were observed, particularly at higher Mg^{2+} concentrations and extended incubation times (Figure 4.14).

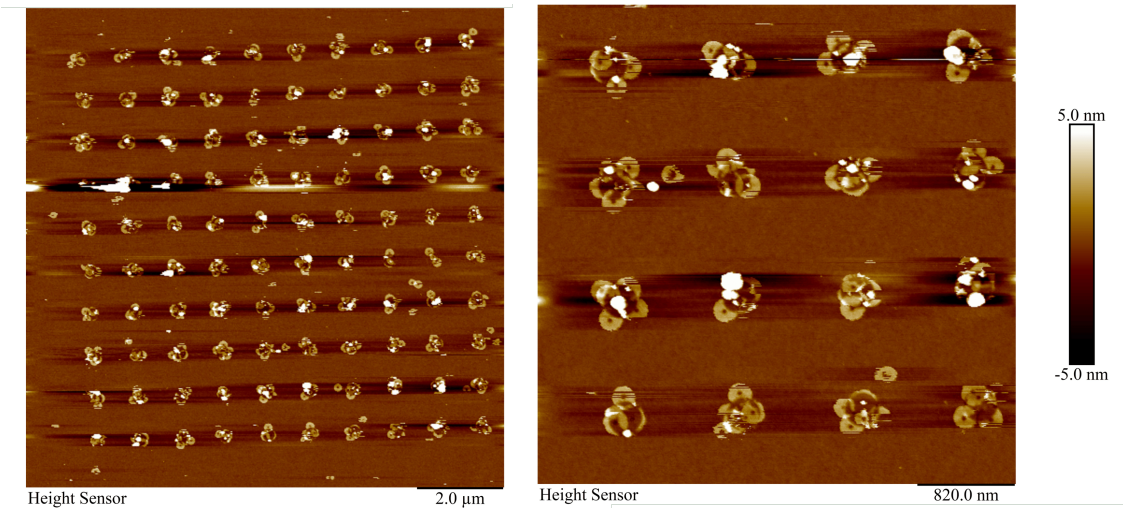

Figure 4.14: AFM images of stacking during origami deposition. In the right image, multiple origami can be seen binding to a single binding site, often stacking over each other.

Origami Design Modifications

Initial attempts to mitigate aggregation involved increasing the origami size to better fit the patterned area. A 4x4 origami design was considered; however, due to low synthesis yield, hexagonal tiles were selected to match the circular pattern shapes more effectively, as seen in Figure 4.15a).

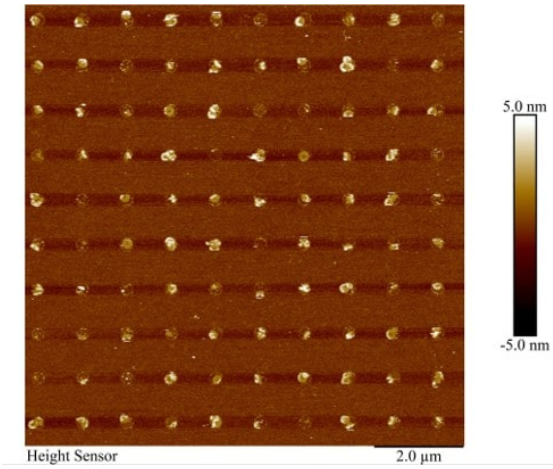

(a) Alignment of pattern size minimizes aggregation while maintaining high occupancy.

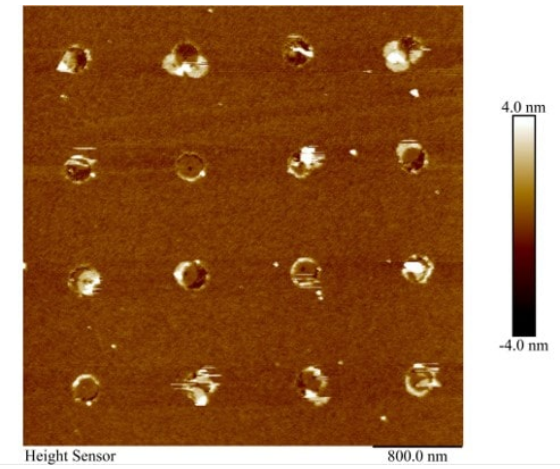

(b) Zoomed-in view of origami alignment with optimized deposition site size.

Figure 4.15: AFM images showing optimization between pattern size and hexagonal tiles. (a) Tile shape modifications fit patterned area more effectively. (b) Optimized PR exposure closely matches pattern size to hexagon size, reducing multiple binding per site.

Other modifications were also made to the hexagonal origami tile to mitigate observed aggregation and stacking, and address the occasional breakdown of the tile, detailed in Section 4.1.

Lithographic Parameter Optimization

Further mitigation of aggregation was pursued by adjusting photolithographic parameters. By refining photoresist exposure dosage and development (Section 4.2), pattern size was more closely aligned with hexagonal tile dimensions, minimizing multi-tile occupancy, as shown in Figure 4.15b. Doing so reduced the likelihood of multiple origami structures interacting with a single site, contributing to an overall improvement in single-origami occupancy.

Drying and Post-Processing Analysis

During the investigation of stacking, a discrepancy was observed between fluid-phase and air-phase imaging. Significant folding, detachment, and aggregation were noted post-drying,

likely due to the destabilization of origami-substrate bonds during drying.

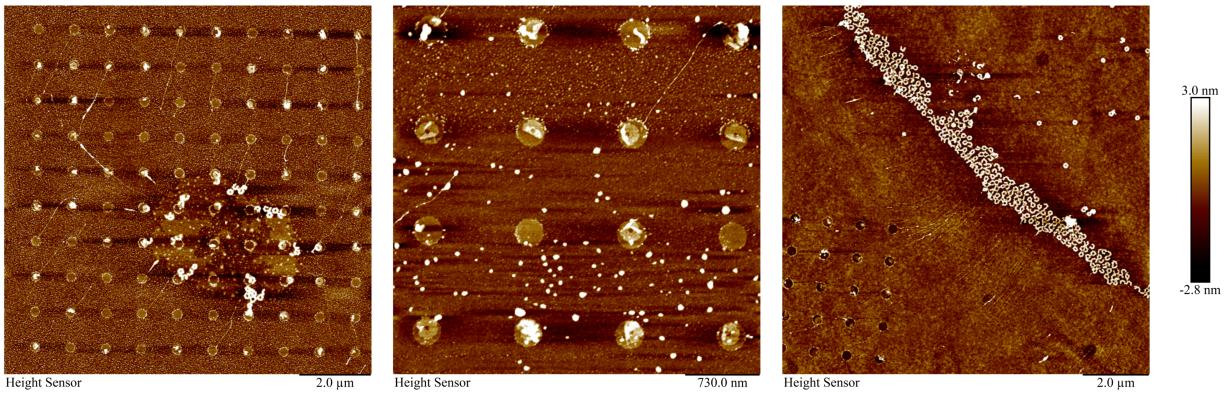

Figure 4.16: Effects of drying on origami placement. We observed low occupancy and detachment (left), folding via lift-off (middle), and aggregation in the drying direction (right).

Various drying techniques were evaluated to address the observed placement and yield inconsistencies. The proposed approaches included:

- Sequential immersions in ethanol at varying concentrations (25%, 50%, 70%, 80%, 90%), each for 10 seconds, followed by air drying.
- Immersion in deionized water for 1 minute, repeated twice.
- A 10-second immersion in a 1:9 ethanol-to-water solution, followed by two 1-minute DI water immersions.

Despite these attempts, none of the drying methods significantly improved yield or placement fidelity. As a result, the drying step was eliminated, and all subsequent imaging was conducted in fluid to maintain origami-substrate interactions and prevent disruptions.

Buffer and Deposition Parameter Optimization

Throughout the optimization of origami design, lithographic parameters, and surface treatments, buffer and deposition parameters were simultaneously adjusted to further control aggregation, stacking, and placement fidelity. The following parameters were tested in 5 mM Tris buffer, which included:

- **DNA Origami Concentration:** Adjusting the concentration controls how much free origami is present for placement. Excess origami increases stacking and aggregation, while lower concentrations reduce multi-layer interactions but may limit binding.

- **Mg^{2+} Concentration:** $MgCl_2$ facilitates electrostatic bridging between DNA and silicon oxide through ion correlation forces. Excessive concentrations (¿15 mM) cause origami deformation or balling up. The effect of increasing concentration is demonstrated in Figure 4.17.

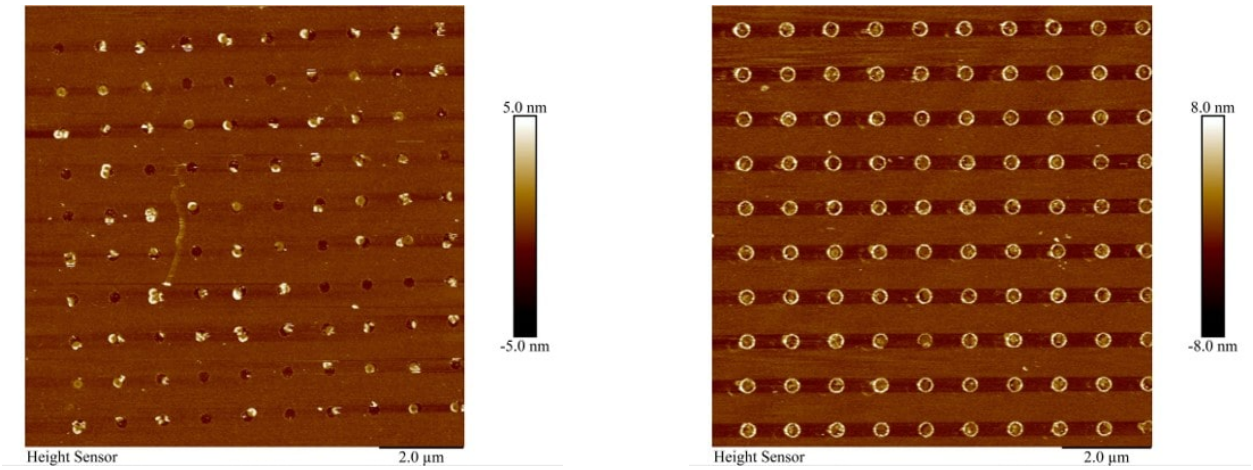

(a) 6mM $MgCl_2$ exhibits sparse occupancy.

(b) 10mM $MgCl_2$ exhibits higher occupancy.

Figure 4.17: Illustrating effect of Mg^{2+} on deposition (100pM DNA 4hr).

- **NaCl Concentration:** NaCl modulates electrostatic screening, competing with Mg^{2+} for charge stabilization, weakening Mg^{2+}-mediated DNA-substrate bridges. Excessive concentrations can destabilize origami-substrate bonds, as Figure 4.18 shows.
- **Incubation Time:** Adjusting incubation times can allow more time for the origami to bind to the surface, increasing binding yield. However, it may also promote aggregation and stacking post-saturation. Figure 4.19 illustrates the effect of raising incubation time.
- **Incubation Temperature:** Higher temperatures increase kinetic energy and may encourage origami to reorient until it forms the most favorable bond. However, excessive heat can also destabilize and denature the DNA origami structure.
- **Buffer pH:** pH affects the charge states of silicon oxide and DNA, influencing electrostatic interactions. Overly acidic conditions can reduce surface negativity (Si–OH $\rightarrow$ Si–OH_2^+), weakening Mg^{2+} bridging. Overly basic conditions increase negative charge on DNA and silicon, but can also weaken Mg^{2+} bridging by precipitation as insoluble $Mg(OH)_2$.

Table 4.2 summarizes the current optimal parameters. This set of parameters exhibited $\sim$95% occupancy (aggregated/stacking included), and between 10-15% single origami occupancy (Figure 4.20b).

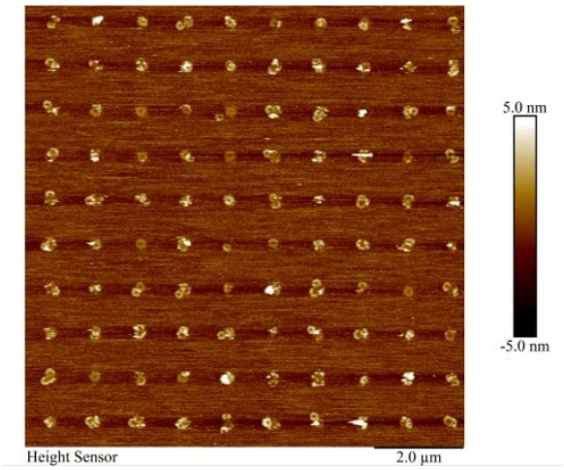

(a) 20mM NaCl exhibits good occupancy with strong ion bridge.

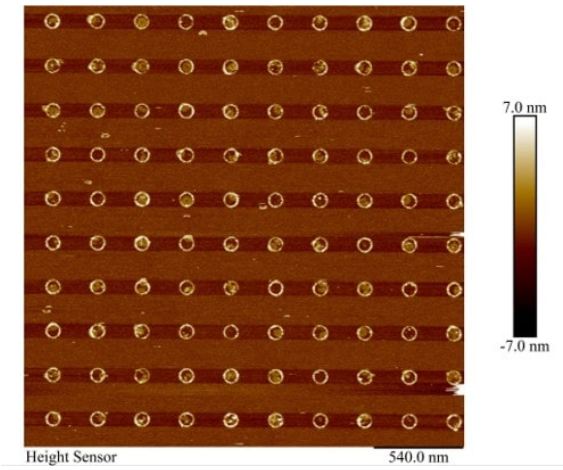

(b) 40mM NaCl exhibits reduced occupancy due to weakened ion bridge.

Figure 4.18: Illustrating effect of NaCl on deposition (10mM Mg 100pM DNA 4hr).

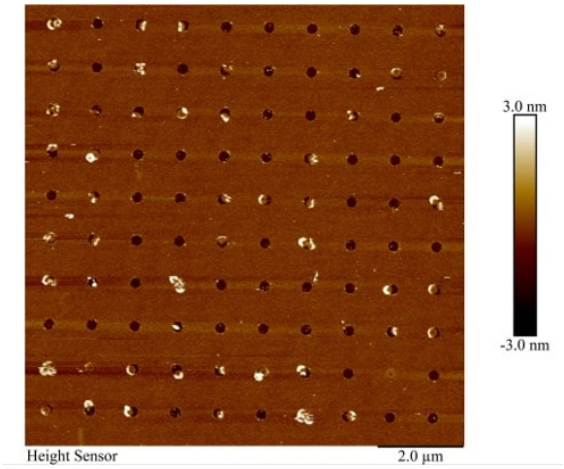

(a) 2hr exhibits lower occupancy.

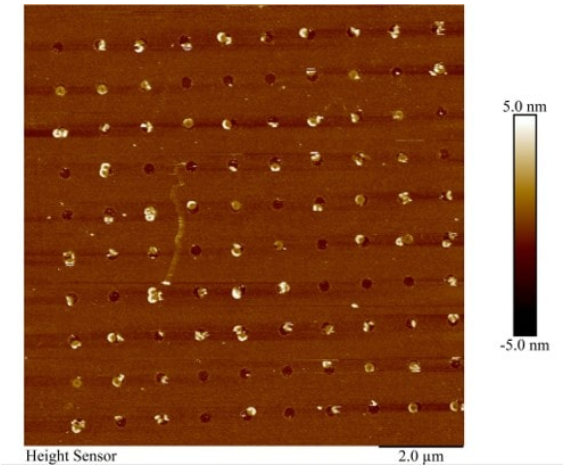

(b) 4hr exhibits improved occupancy.

Figure 4.19: Illustrating effect of incubation time on deposition (6mM Mg 100pM DNA).

Table 4.2: Current Optimized Buffer and Deposition Parameters

Parameter	Tested Range	Current Optimal
DNA Origami Concentration	100 pM – 1 nM	100 pM
$MgCl_2$ Concentration	4 – 50 mM	10 mM
NaCl Concentration	0 – 100 mM	20 mM
Incubation Time	30 min – 4 h	4 h
Incubation Temperature	RT – 30°C	RT
Buffer pH	8 – 9	8.35, 8.9

Benchmarking and Future Work

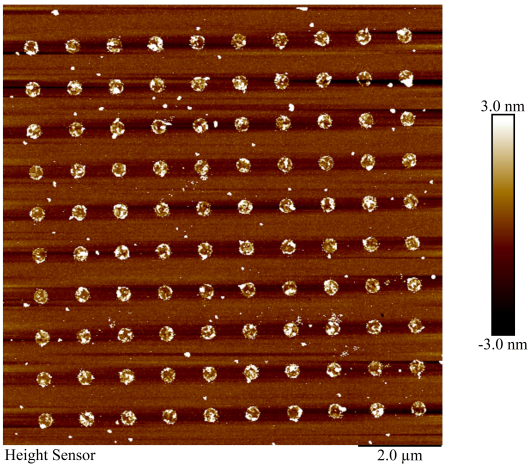

(a) Pre-optimization deposition exhibited significant folding, aggregation, and poor binding quality.

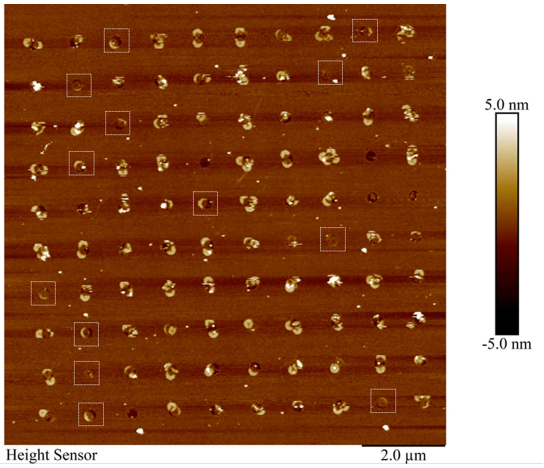

(b) Optimized deposition achieves 95% pattern occupancy, and 13% single origami occupancy.

Figure 4.20: Comparison between initial deposition results and current optimal deposition.

Figure 4.20 illustrates the progression from initial deposition conditions to the current optimized parameters, highlighting significant binding quality and yield improvements. However, vertical stacking remains a persistent challenge despite achieving a 95% occupancy yield, with multi-tile assemblies still occurring at some patterned sites.

Further parameter optimization is necessary to disrupt the bonds between stacked origami and fully achieve single-origami occupancy across all sites. Potential strategies to address stacking include:

- Lowering placement buffer pH from 8.35 to 8.0 to reduce electrostatic attraction between DNA origami tiles and minimize multi-layer assembly.
- Implementing pulsed Mg^{2+} concentration cycles to weaken bridging interactions transiently, disrupting stacked tiles without dislodging bound origami.
- Incremental ramping of NaCl concentration (0–50 mM) to selectively screen electrostatic interactions, destabilizing stacked assemblies while preserving single-tile binding.

While much remains to be explored, the progress achieved thus far is encouraging. With systematic testing of these parameters, we are optimistic that further refinements will convert the current 95% occupancy yield to exclusively single-origami occupancy across all patterned sites, effectively eliminating multi-layer assemblies.

Chapter 5

Conclusion and Discussion

In this thesis, we extended the foundational work of Gopinath et al. by exploring the integration of DNA origami with photolithographically patterned silicon surfaces. Focusing on parameter tuning, we aimed to optimize the placement yield and spatial precision of DNA nanostructures through site-specific deposition using fractal-assembled DNA origami tiles, thereby bridging bottom-up self-assembly with top-down lithographic techniques.

Our comparative analysis of electrostatic and thermodynamic binding strategies revealed that while electrostatic interactions facilitate rapid binding, thermodynamic approaches provide more consistent spatial control, particularly for complex nanostructures. This analysis underscores the need to optimize binding strategies further to balance yield and precision. Refining tile designs and surface modifications could also enhance selective binding and spatial control. These advancements could enable more complex, multi-layered nanostructures and more precise patterning of DNA assemblies on semiconductor substrates.

Beyond demonstrating the potential for precise placement, the frameworks developed in this work hold promise for various applications. Optimized DNA origami placement could enable nanoscale patterning for biosensing and programmable nanosystems. Extending these methods to multi-layered assemblies could further expand their utility in complex sensing arrays, where spatial accuracy and site-specific functionalization are crucial.

By systematically examining how tile geometry, surface chemistry, and binding modality influence placement outcomes, this work provides valuable insights for scaling DNA nanofabrication toward more programmable and robust nanofabrication methods that effectively bridge molecular self-assembly with semiconductor manufacturing.

Bibliography

[1] B. Babatunde et al. "Generating DNA Origami Nanostructures through Shape Annealing". In: *Applied Sciences* 11.7 (2021), p. 2950. DOI: https://doi.org/10.3390/app11072950. URL: https://doi.org/10.3390/app11072950.

[2] Ashwin Gopinath et al. "Engineering and mapping nanocavity emission via precision placement of DNA origami". In: *Nature* 535.7612 (2016), pp. 401–405. DOI: 10.1038/nature18287.

[3] Zhimei He et al. "Self-assembly of DNA origami for nanofabrication, biosensing, drug delivery, and computational storage". In: *iScience* 26.9 (2023), p. 10715. DOI: 10.1016/j.isci.2023.10715.

[4] Ryan J. Kershner et al. "Placement and orientation of individual DNA shapes on lithographically patterned surfaces". In: *Nature Nanotechnology* 4.9 (2009), pp. 557–561. DOI: 10.1038/nnano.2009.220.

[5] Myoungseok Kim. "Development of programmable nanoscale origami through self-assembled DNA wireframe structures". Master's thesis. MA thesis. Seoul, South Korea: Seoul National University, Department of Mechanical Engineering, 2022.

[6] Paul W. K. Rothemund. "Folding DNA to create nanoscale shapes and patterns". In: *Nature* 440.7082 (2006), pp. 297–302. DOI: 10.1038/nature04586.

[7] Grigory Tikhomirov, Philip Petersen, and Lulu Qian. "Fractal assembly of micrometre-scale DNA origami arrays with arbitrary patterns". In: *Nature* 552.7683 (2017), pp. 67–71. DOI: 10.1038/nature24655.

[8] Grigory Tikhomirov, Philip Petersen, and Lulu Qian. "Triangular DNA Origami Tilings". In: *Journal of the American Chemical Society* 140.49 (2018), pp. 17361–17364. DOI: 10.1021/jacs.8b10609.

[9] Beihang Yu et al. "Nanopatterned Monolayers of Bioinspired, Sequence-Defined Polypeptoid Brushes for Semiconductor/Bio Interfaces". In: *ACS Nano* 18.10 (2024), pp. 7411–7423. DOI: 10.1021/acsnano.3c10204.